Vaccine Discovery and Development: Lessons from COVID-19

Free eBook

Emerging infectious diseases (EIDs) can evolve into a global healthcare crisis or pandemic. Scientists have previously required years to develop vaccines or therapeutics. The use of high throughput technology can greatly broaden the insights collected during discovery, augment efficiency and safety of handling EIDs, and shorten timelines.

Download this publication for an overview of many lessons learned in virology, immunology, and vaccine research during COVID-19 vaccine development.

Download here

SARTORIUS

CURRENT PROTOCOLS
A Wiley Brand

RESEARCH ARTICLE

Fibroblast growth factor induced *Ucp1* expression in preadipocytes requires PGE2 biosynthesis and glycolytic flux

Thomas Gantert[1] ID | **Fiona Henkel**[2] | **Christine Wurmser**[3] | **Josef Oeckl**[1] | **Lena Fischer**[1] | **Mark Haid**[4] | **Jerzy Adamski**[4,5,6,7] | **Julia Esser-von Bieren**[2] | **Martin Klingenspor**[1,8,9] ID | **Tobias Fromme**[1]

[1]Department of Molecular Nutritional Medicine, TUM School of Life Sciences, Technical University of Munich, Freising, Germany

[2]Center of Allergy and Environment (ZAUM), Helmholtz Center Munich, Technical University of Munich, Munich, Germany

[3]Department of Animal Breeding, TUM School of Life Sciences, Technical University of Munich, Freising, Germany

[4]Research Unit Molecular Endocrinology and Metabolism, Helmholtz Center Munich, German Research Center for Environmental Health, Neuherberg, Germany

[5]German Center for Diabetes Research (DZD), Neuherberg, Germany

[6]Institute of Experimental Genetics, Center of Life and Food Sciences Weihenstephan, Technical University of Munich, Freising, Germany

[7]Department of Biochemistry, Yong Loo Lin School of Medicine, National University of Singapore, Singapore, Singapore

[8]EKFZ—Else Kröner-Fresenius Center for Nutritional Medicine, Technical University of Munich, Freising, Germany

[9]ZIEL—Institute for Food & Health, Technical University of Munich, Freising, Germany

Correspondence
Tobias Fromme and Thomas Gantert, Department of Molecular Nutritional Medicine, TUM School of Life Sciences, Technical University of Munich, Gregor-Mendel-Str. 2, Freising 85354, Germany.
Email: fromme@tum.de (T. F.) and thomas.gantert@tum.de (T. G.)

Funding information
German Research Foundation, Grant/Award Number: FR 3628/2-1

Abstract

High uncoupling protein 1 (*Ucp1*) expression is a characteristic of differentiated brown adipocytes and is linked to adipogenic differentiation. Paracrine fibroblast growth factor 8b (FGF8b) strongly induces *Ucp1* transcription in white adipocytes independent of adipogenesis. Here, we report that FGF8b and other paracrine FGFs act on brown and white preadipocytes to upregulate *Ucp1* expression via a FGFR1-MEK1/2-ERK1/2 axis, independent of adipogenesis. Transcriptomic analysis revealed an upregulation of prostaglandin biosynthesis and glycolysis upon Fgf8b treatment of preadipocytes. Oxylipin measurement by LC-MS/MS in FGF8b conditioned media identified prostaglandin E_2 as a putative mediator of FGF8b induced *Ucp1* transcription. RNA interference and pharmacological inhibition of the prostaglandin E_2 biosynthetic pathway confirmed that PGE2 is causally involved in the control over *Ucp1* transcription. Importantly, impairment of or failure to induce glycolytic flux blunted the induction of *Ucp1*, even in the presence of PGE_2. Lastly, a screening of transcription factors identified *Nrf1* and *Hes1* as required regulators of

---

Abbreviations: 2-DG, 2-deoxy-D-glucose; BAT, brown adipose tissue; *C/EBPs*, CCAAT- enhancer-binding proteins; *Cox2*, cyclooxygenase 2; ECM, extracellular matrix; *Erk1/2*, mitogen-activated protein kinase 1/2; *Fgf*, fibroblast growth factor; *Hes1*, hairy and enhancer of split 1; *Hk2*, hexokinase 2; *Ldha*, lactate dehydrogenase A; *Mek1/2*, mitogen-activated protein kinas kinase 1/2; *Nrf1*, nuclear respiratory factor 1; NST, non-shivering thermogenesis; *Pgc1a*, proliferator-activated receptor gamma coactivator 1α; PGE2, prostaglandin E2; PGI2, prostaglandin I2; *Ppar*, Peroxisome proliferator-activated receptors; *Prdm16*, PR domain–containing protein 16; *Ptges1*, prostaglandin E2 synthase 1; *Ptgis*, prostaglandin I2 synthase; *Ptgs1/2*, prostaglandin endoperoxidase 1/2; *Slc2a1*, glucose transporter 1; SVF, stromal-vascular fraction; *Ucp1*, uncoupling protein 1; WAT, white adipose tissue.

FGF8b induced *Ucp1* expression. Thus, we conclude that paracrine FGFs co-regulate prostaglandin and glucose metabolism to induce *Ucp1* expression in a *Nrf1/Hes1*-dependent manner in preadipocytes, revealing a novel regulatory network in control of *Ucp1* expression in a formerly unrecognized cell type.

KEYWORDS

Fgf signaling, Fgf8, glucose metabolism, glycolysis, paracrine fibroblast growth factor, PGE$_2$, preadipocyte, prostaglandin, Ucp1, uncoupling protein 1

1 | INTRODUCTION

Non-shivering thermogenesis (NST) in mammals describes a process in which chemical energy is dissipated as heat within thermogenic organs.[1,2] These organs are most prominently brown adipose tissue (BAT), but also "browned" white adipose tissue (WAT). Their functional, cellular entities are the brown and beige adipocyte, respectively.[3-5] Brown and beige adipocytes are characterized by multilocular lipid droplets, high mitochondrial content and high abundance of the heat producing protein Uncoupling protein 1 (UCP1). Residing in the mitochondrial inner membrane, UCP1 dissipates the proton gradient generated by the electron transport chain, thus uncoupling ATP production from oxygen consumption. This futile cycle contributes to whole body energy balance and is thus able to reduce fat mass in rodent models of obesity.[6,7] In the light of these findings, the presence of active BAT in humans has garnered much interest due to its therapeutic implication in combatting the global obesity pandemic.[4,8-10]

Ucp1 gene expression in brown/beige adipocytes cells is tightly regulated by transcriptional networks governed by adipogenic and thermogenic regulators such as peroxisome proliferator-activated receptor γ (PPARγ), CCAAT- enhancer-binding proteins (C/EBPs), PR domain–containing protein 16 (PRDM16) and proliferator- activated receptor gamma coactivator 1-alpha (PGC1a).[1,11] The canonical signaling pathway to induce thermogenic activity and differentiation is initiated by binding of noradrenaline to the β3-adrenoreceptor, but other endogenous hormones have been studied, including the endocrine acting fibroblast growth factor 21 (FGF21).[12,13] FGF21 belongs to the fibroblast growth factor family, a large group of 22 structurally related peptides which can be classified into three subgroups: paracrine, endocrine, and intracrine FGFs depending on their mode of action.[14,15] Paracrine and endocrine FGFs signal through cell surface tyrosine kinase receptors encoded by four FGF-receptor genes (*Fgfr1-4*) to exert their pleiotropic biological functions such as controlling cell proliferation, differentiation, regeneration, tissue repair, and metabolism.[16-18] Additionally, receptor activation requires binding of paracrine FGFs to heparin/heparan sulfate proteoglycans (HSPGs) which serve as cofactors, while endocrine FGFs bind to members of the Klotho family. Formation of the FGF-FGFR-cofactor ternary complex activates various signaling cascades including MAPK, PI3K-AKT, STAT and PLCγ-PKC pathways.[14] Surprisingly, even though FGF21 has been intensively studied as a potential regulator of thermogenic differentiation,[19] paracrine FGFs have been largely ignored, despite their known role in the regulation of cell fate decisions. There have been notable exceptions for some of the paracrine FGFs in recent years, such as for FGF6,[20] FGF9,[20,21] FGF16[22] and our own work on FGF8b.[23]

FGF8 was originally identified as an androgen-induced growth factor in conditioned media of the mouse mammary cancer cell line SC-3.[24] Unlike most FGFs, FGF8 is subject to alternative splicing which gives rise to eight murine (FGFa-h) and four human (FGFa, b, e, f) protein isoforms.[25,26] The dominant function of these isoforms was ascribed to the FGF8b isoform, which has the highest transforming potential of NIH3T3 cells across all isoforms.[27,28] The mouse and human FGF8b isoform share 100% protein sequence identity. FGF8b controls a plethora of biological processes during early and late embryogenesis by orchestrating the growth and patterning of a multitude of tissues and organs in the embryo.[27] In the adult mouse *Fgf8* mRNA expression is mostly restricted to the ovary and testes.[29]

In our previous work, we compared the capacity of all 15 paracrine FGFs to induce *Ucp1* expression in white adipocytes in cell culture and identified FGF8b to be the most effective.[23] Treatment of white adipocytes with FGF8b during differentiation was associated with a distinct suppression of adipogenesis, as reported for other paracrine FGFs before.[20,21] This led us to hypothesize that undifferentiated preadipocytes are the source of significant *Ucp1* expression via a non-classical pathway, offering the unique opportunity to investigate *Ucp1*-specific gene regulation without overlay of the adipogenic transcriptional program.

The aim of our present study is to validate the *Ucp1* inducing property of FGF8b in brown and white preadipocytes and elucidate the FGF8b-specific signal transmission from the receptor level to the underlying signaling pathway and ultimately to potential metabolic and transcriptional regulators. We found that FGF8b strongly upregulated *Ucp1* gene expression in both white and brown preadipocytes, uncovered the responsible receptor and signaling cascade, and

identified an essential role of prostaglandin E_2 production, glycolytic flux and the transcriptional regulators *Nrf1/Hes1* in controlling gene expression of *Ucp1*.

2 | MATERIAL AND METHODS

2.1 | Cell culture

Brown and white immortalized and primary preadipocytes— the term 'preadipocyte' in this context refers to the stromal-vascular fraction, which is a mixture of several cell types, the most dominant of which is the preadipocyte fraction—were cultured in standard media containing Dulbecco's modified Eagle's medium with 4.5 g/L glucose (Sigma-Aldrich) supplemented with 10% fetal bovine serum (Biochrom) and antibiotics (40 IU/mL penicillin, 40 µg/mL streptomycin, 40 µg/mL gentamycin) at 37°C in a humidified atmosphere. Preadipocytes were treated with recombinant fibroblast growth factor (FGF) 8b, FGF1, FGF6, FGF9 and FGF21 when confluence reached 80%-90%. Heparin (H3149-10KU, Sigma-Aldrich), a cofactor of FGF signaling, was used in a concentration of 1 µg/mL to amplify signaling activity. To evaluate the proliferative effect of growth factors, treated preadipocytes were trypsinized and counted on an automated cell counter (TC20, Biorad). The cytotoxicity of the glucose uptake inhibitor treatment with BAY-876 was evaluated using the CytoTox-Fluor assay kit (Promega) according to the manufacturer's instructions.

Differentiation of preadipocytes was induced by supplementing standard media with 125 µM indomethacin, 500 µM 3-isobutyl-1-methylxanthine, 1 µM dexamethasone, 1 nM T_3, 850 nM insulin and 1 µM rosiglitazone. Fresh differentiation media containing 1 nM T_3, 850 nM insulin, 1 µM rosiglitazone with or without 125 ng/mL FGF8b + 1 µg/mL heparin was changed every other day for the next six days. Neutral lipid staining was performed with 3 µg/mL of the fluorescent lipophilic dye BODIPY 493/503 (Invitrogen) in PBS for 20 minutes at RT and fluorescence images were acquired on a fluorescence microscope (ex/em: 488-503/515-545, Leica DMI6000B).

For the generation of immortalized cell lines, retrovirus particles were produced by calcium phosphate transfection of the packaging cell line Bosc-23 with pBABE-puro SV40 LT, a vector encoding for the simian virus 40 large T antigen. The stromal-vascular fractions (SVF) of seven week-old male *Ucp1*-reporter (C57BL/6N),[30] 129S6Sv/Ev Tac, and *Ucp1*-knock-out mice (129S) were isolated by collagen digestion of minced brown and white inguinal adipose tissue of 3-4 mice. Primary cells were grown to 60%-70% confluence and transduced with sterile filtered retroviral supernatant mixed with 2 µg/mL polybrene. Immortalized brown and white preadipocytes were selected with 2 µg/mL puromycin for 2 weeks and aliquots were stored in liquid nitrogen until use.

2.2 | Chemicals

Recombinant mouse fibroblast growth factor 1 (FGF1), epidermal growth factor (EGF), platelet-derived growth factor (PDGF-BB) and mouse/human FGF8b were purchased from PeproTech. Recombinant mouse FGF6, FGF9 and FGF21 were purchased from R&D Systems. Most inhibitors used for probing different signaling pathways, including LY2874455 (FGF-receptor phosphorylation), SH-4-54 (Stat 3, 5), TAK632 (pan-RAF), Trametinib (MEK1/2), SCH772984 (ERK1/2), SB202190 (p38MAPK) and Wortmannin (PI3K) were purchased from Biotrend. Inhibitors bisindolylmaleimide I (pan-PKC), diclofenac (COX1, COX2) and celecoxib (COX2), BAY-876 (GLUT1), sodium oxamate (LDH-A), GW6471 (PPARα), GSK3787 (PPARβ/δ), GW9662 (PPARγ), CAY10678, CAY10526 (PTGES1) and U-51605 (PTGIS) were purchased from Caymen Chemical. Prostaglandin E2 was purchased from Caymen Chemical.

2.3 | Lentiviral overexpression of fibroblast growth factor 8b

The overexpression construct was cloned by substituting the open reading frame (ORF) of green fluorescent protein (EGFP) in pLenti c-MYC-DDK-Puro-GFP (gift from Giovanni Tonon, Addgene #123299 as published[31]) with the human FGF8b ORF in pCMV6-FGF8b (Origene, RC214620). Lentiviral particles were produced by co-transfection of HEK-293T cells with pLenti c-MYC-DDK-GFP or pLenti c-MYC-DDK-Puro-FGF8B and second generation packaging plasmids (psPAX2 + pMD2.G) using PolyFect transfection reagent (Qiagen). Lentivirus in cell culture supernatant was concentrated (PEG-it Virus Precipitation Solution, Biocat) and titer determined (One-Wash Lentivirus Titer Kit, HIV-1 p24 ELISA, Origene). Immortalized brown preadipocytes (5×10^4 cells) were transduced with lentivirus (multiplicity of infection = 1000) and 8 µg/mL polybrene for 16 hours. Cells were cultured in 1 µg/mL heparin containing standard media for 4 days before harvest.

2.4 | RNA isolation, cDNA synthesis and RT-qPCR

Harvested cells were lysed in TRIsure reagent (BIO-38033, Bioline) and total RNA was isolated by column elution (SV Total RNA Isolation System, Promega). RNA concentration was measured spectrophotometrically (Nanodrop-1000) and

reverse transcribed into cDNA (SensiFast cDNA Synthesis Kit, Bioline). Real-time quantitative polymerase chain reaction (RT-qPCR) was performed on a LightCycler480 Real-Time PCR System (Roche) using SensiMix SYBR No-ROX Kit (Bioline) and quantified by the relative standard curve method employing standards from pooled sample cDNAs. Relative transcript abundances of target genes were normalized to the abundance of the reference gene general transcription factor IIB (*TfIIb*). Primer sequences are listed in Table S1.

2.5 | Protein isolation and immunoblotting

Harvested cells were lysed in radio-immunoprecipitation-assay (RIPA) buffer (50 mM Tris-Cl, 1% [v/v] NP-40, 0.25% [w/v] sodium deoxycholate, 150 mM NaCl, 1 mM EDTA, 1:1000 protease inhibitor [P8340-Sigma]), incubated on ice for 30 minutes and spun down for 15 minutes at max speed in a table top centrifuge at 4°C. Protein concentration in cell lysate supernatant was measured with the Pierce BCA Assay Kit (Thermo Scientific). Cell lysate in Laemmli buffer (33 mM Tris-HCl, pH 6.8, 5% SDS, 25% (w/v) glycerol, 0.01% bromophenol blue) were subjected to SDS-PAGE on 4%-20% Mini-PROTEAN TGX Stain-Free precast gels (Biorad) and subsequently proteins were blotted onto a nitrocellulose membrane. Membranes were blocked in 3% (w/v) bovine serum albumin in Tris-buffered saline (TBS) and incubated overnight at 4°C with primary antibodies rabbit anti-UCP1 (ab23841, Abcam), rabbit anti-FGFR1 (#9740, Cell Signaling Technology) and mouse anti-β-Actin, clone C4 (MAB1501, Merck Millipore). Then, membranes were washed with TBS-0.1% Tween-20 before and after incubation with secondary antibodies IRDye 800CW goat anti-rabbit and IRDye 680CW donkey anti-mouse for 1 hour at room temperature. Secondary antibodies were washed off with TBS-0.1% Tween-20 and rinsed once with TBS without Tween-20. Images were acquired on the Odyssey Infrared Imaging System (LI-COR) and analyzed with the Image Studio Lite Software (LI-COR) v.5.2.

2.6 | Next-Generation Sequencing (NGS)

Global gene expression levels were assessed by transcriptomic analysis. The first sequencing experiment was based on immortalized brown and white preadipocytes from the *Ucp1*-reporter mouse model (C57BL/6N) treated with or without 125 ng/mL FGFb + 1 μg/mL heparin, for 48 hours in four replicates per group. The second sequencing experiment was based on immortalized brown preadipocytes from 129S6Sv/Ev Tac mice treated with equimolar concentrations (5.55 nM) of either FGF1, FGF9 or FGF8b and a FGF8b group co-incubated with 2 μM of the glucose transporter 1 inhibitor BAY-876. Treatment lasted for 48 hours with 1 μg/

mL heparin in all groups with three replicates per group. Total RNA was isolated, followed by cDNA library preparation of 500 ng/sample using the TruSeq Stranded mRNA Library Prep (20020594, Illumina GmbH) and TruSeq RNA Single Indexes Set A (20 020 492, Illumina GmbH). The sequencing was performed on an Illumina HiSeq2500 instrument using a HiSeq Rapid SR Cluster Kit v2 (GD-402-4002, Illumina GmbH) and HiSeq Rapid SBS Kit v2 (FC-402-4022, Illumina GmbH) for cluster generation and synthesis by sequencing, respectively. Run parameters were multiplexed single indexed (7 cycles) single-end-reads (50 cycles) with a read depth of >22 M reads per sample. Software employed included HiSeq control software 2.2.70 for sequencing, Real-Time Analysis (RTA) 1.18.66.4 for image analysis and base calling and bcl2fastq conversion software v2.20 for fastq-file generation. Reads were mapped using the Genomatix Mapping tool which is implemented in the Genomatix Software Suite and allowed for mapping against the Genomatix proprietary ElDorado genome annotation database (2013). Differential expression analysis was performed on RefSeq identified transcripts using the *DESeq2* package in R version 3.6.3.

2.7 | Metabolite measurements

Lactate in cell culture supernatant was assayed in the presence of hydrazine at alkaline pH and was based on the spectrophotometric measurement of NADH at 340 nm formed by lactate dehydrogenase (10127230001, Roche). Glucose in cell culture supernatant was mixed with glycerol in a volume-to-volume ratio of 60:40 and was then determined with a glucometer (FreeStyle Lite, Abbott). Glucose uptake was measured in a non-radioactive, plate-based format based on the detection of 2-deoxyglucose-6-phosphate (2-DG6P) by a luciferase-coupled reaction (Glucose Uptake-Glo Assay, Promega). Brown preadipocytes (129S) were stimulated with FGF8b for 48 hours, incubated in glucose-free medium for 2 hours and stimulated with 2.5 mM 2-DG for 20 minutes until lysis and quantification on a luminometer (Berthold Detection Systems).

2.8 | Bioluminescence quantitation

Luciferase activity was assayed as a surrogate measure for *Ucp1* expression (*Ucp1*-LUC) in cell lysates derived from the *Ucp1*-reporter mouse model.[30] Samples were measured on a Sirius single tube luminometer (Berthold Detection Systems) using the luciferase assay system kit (E1501, Promega). Briefly, after removing cell culture medium, cells were washed with phosphate buffered saline (PBS) and then incubated in cell culture lysis reagent for 15 minutes on a horizontal shaker. 10 μL of cell lysate was then mixed with 50 μL luciferase assay buffer in a 5 ml polystyrene tube before luminescence quantitation.

Readouts were normalized to protein concentrations (Pierce BCA Assay Kit, Thermo Scientific).

2.9 | Gene silencing by dicer-substrate short interfering RNAs

Gene silencing of target genes in preadipocytes was achieved using dicer-substrate short interfering RNAs (dsiRNAs, Integrated DNA Technologies). Briefly, transfection reagent (Lipofectamine RNAiMAX, Thermo Fisher Scientific) and dsiRNA (final concentration 20 nM) were diluted in Opti-MEM reduced serum medium, mixed in a 1:1 ratio and incubated for 20 minutes at room temperature. A non-targeting scrambled dsiRNAs was used as negative control (51-01-19-09, Integrated DNA Technologies). Preadipocytes were added to the transfection mixture using a reverse transfection approach. Knockdown efficiency was assessed by qPCR 48 hours post-transfection. Stimulation with 125 ng/mL FGF8b + 1 μg/mL heparin was started 48 hours post-transfection and the effect on *Ucp1* expression was examined 48 hours later by luciferase assay. DsiRNA sequences are listed in Table S2.

2.10 | Glycolysis assay

Oxygen consumption and proton production rates were measured in a glycolysis assay on an Extracellular Flux Analyzer (Seahorse XF96, Agilent Technologies) according to a published protocol.[32] Culture medium was substituted for glucose free assay medium (DMEM Base D5030, 5 mM Hepes, 31 mM NaCl, 2 mM GlutaMAX (Gibco), 0.1% (w/v) free fatty acid free BSA, 15 mg/L phenol red, pH 7.4) 1 hour prior to measurement. Basal glycolytic rate was measured after the addition of 10 mM glucose, enabling ATP production by both oxidative phosphorylation and glycolysis. Subsequently, glycolytic flux was increased by inhibition of respiration with 1 μM rotenone and 1 μM myxothiazol. To assess maximum glycolytic capacity, cellular ATP demand was increased by the addition of 400 μM monensin and 2 μM Carbonyl cyanide 4-(trifluoromethoxy)phenylhydrazone (FCCP). Contribution of respiratory and glycolytic acidification to total proton production rates were calculated as published.[33]

2.11 | LC-MS/MS lipid mediator analysis

Lipid mediator analysis was performed as described previously.[34] Briefly, cell culture supernatant was collected and centrifuged at 5000 g and 4°C to remove cell debris. Supernatant was then mixed with the same volume of cold MeOH and stored at −80°C until measurement. Automated solid phase extractions were performed with a Microlab STAR robot (Hamilton). Prior to extraction all samples were diluted with H_2O to a MeOH content of 15% and 10 μL of IS stock solution was added. Samples were extracted using Strata-X 96-well plates (30 mg, Phenomenex) and eluted with MeOH. Samples were evaporated to dryness under N_2 stream and redissolved in 100 μL MeOH/H_2O (1:1). Chromatographic separation of oxylipins was achieved with a 1260 Series HPLC (Agilent) using a Kinetex C18 reversed phase column (2.6 μm, 100 × 2.1 mm, Phenomenex) with a SecurityGuard Ultra Cartridge C18 (Phenomenex) precolumn. The QTRAP 5500 mass spectrometer (Sciex), equipped with a Turbo-VTM ion source, was operated in negative ionization mode. Samples were injected via an HTC PAL autosampler (CTC Analytics), set to 7.5°C. Identification of metabolites was achieved via retention time and scheduled multiple reaction monitoring. Acquisition of LC-MS/MS data was performed using Analyst Software 1.6.3 followed by quantification with MultiQuant Software 3.0.2 (both Sciex). Quality control of the LC-MS/MS analysis was performed by excluding metabolites with a coefficient of variation >20 and those that were present in less than 70% of all measured samples.

2.12 | Statistics

Statistical analyses were performed using GraphPad Prism version 6.07, (GraphPad Software, San Diego, California, USA). Bonferroni corrected parametric tests (Student's *t*-test, one-way and two-way ANOVA) were used to analyze data with approximate normal distribution, otherwise non-parametric tests (Mann-Whitney, Kruskal-Wallis) were used with Dunn's correction. For bioinformatic analyses and statistics of RNA-Sequencing data, the R packages *DESeq2*, *pheatmap*, *ReactomePA* were used in RStudio (R version 3.6.3). Data are presented as means ± SD, except otherwise noted in figure legends. $P < .05$ was considered statistically significant and indicated with asterisks as follows *$P < .05$. **$P < .01$, ***$P < .001$, ****$P < .0001$.

3 | RESULTS

Paracrine FGF8b induces *Ucp1* expression in cultured white epididymal adipocytes, independent of adipogenesis and in the absence of other hallmarks of browning, pointing towards the undifferentiated preadipocyte itself as the surprising origin of significant *Ucp1* expression.[23] We comprehensively validated preadipocyte-specific *Ucp1* expression and its FGF8b dose-response relationship, time course of effect and compared it to other FGFs using immortalized and primary brown and white preadipocytes.

3.1 | FGF8b dose-dependently induces *Ucp1* gene expression in immortalized and primary brown and white preadipocytes

Immortalized brown preadipocytes from 129S6Sv/Ev Tac mice treated with recombinant FGF8b for 72 hours significantly increased *Ucp1* gene expression both on the transcript and the protein level (Figure 1A,B). The induction of *Ucp1* transcription was replicated by lentivirus mediated

overexpression of *Fgf8b* in brown preadipocytes (Figure 1C) and was independent of the employed mouse strain (Figure S1D,E). To characterize the nature of FGF8b mediated *Ucp1* expression in addition to RT-qPCR and immunoblotting, we utilized our recently established luciferase knock-in *Ucp1*-reporter mouse model[30] providing luminescence as a reliable and efficient surrogate measure for *Ucp1* expression. Immortalized brown and white preadipocytes derived from the *Ucp1*-reporter model and treated with FGF8b
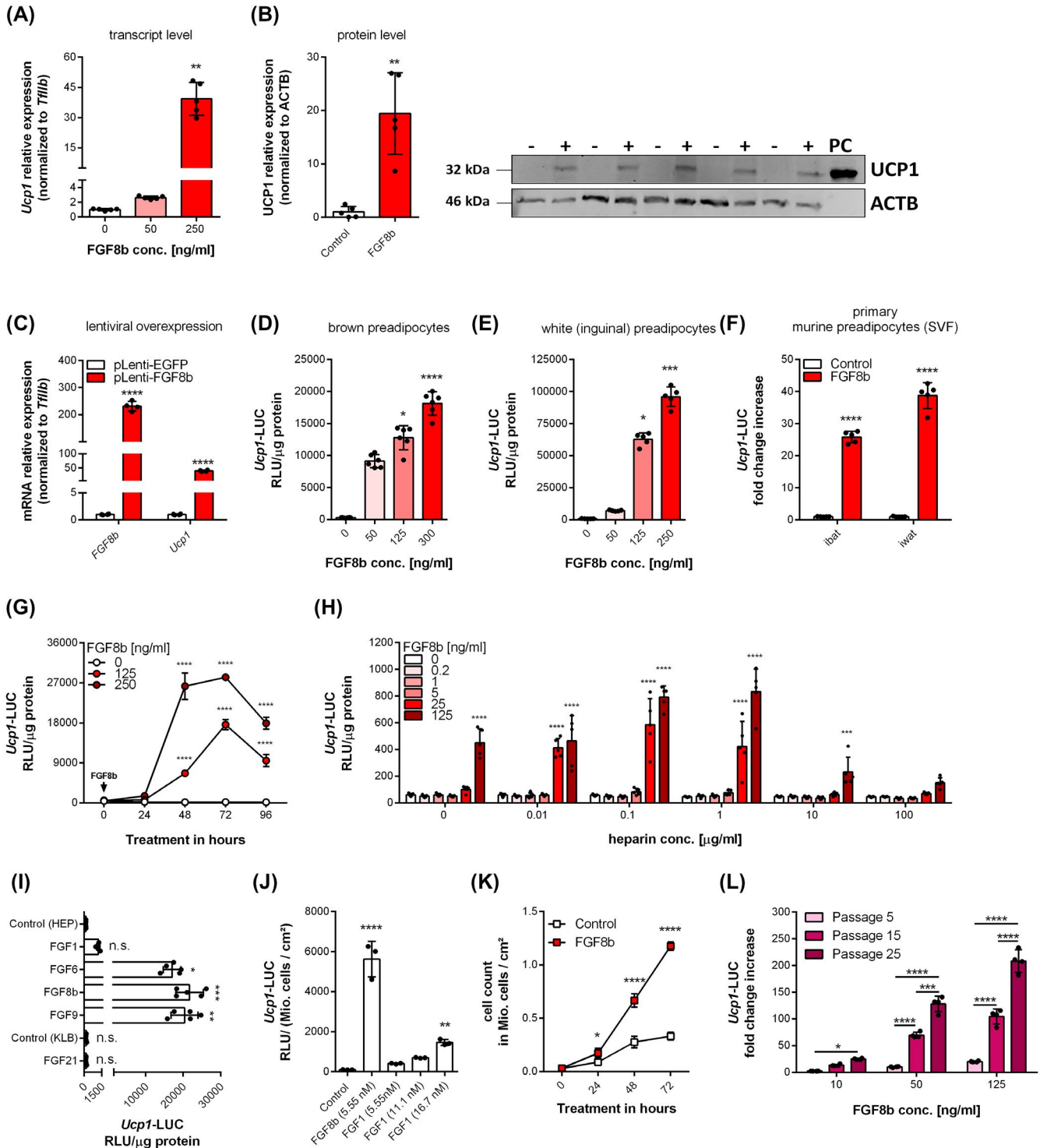
FIGURE 1 FGF8b induces *Ucp1* expression in brown and white preadipocytes. A, *Ucp1* mRNA expression in brown preadipocytes from 129S6Sv/Ev Tac mice treated with FGF8b for 48 h (N = 5 per group). B, UCP1 protein expression in brown preadipocytes from 129S6Sv/Ev Tac mice treated with 250 ng/mL FGF8b for 72 h. Control group; + FGF8b group; iBAT tissue positive control (PC) (N = 5 per group). C, Lentiviral overexpression of human FGF8b and EGFP in brown preadipocytes cultured for 4 days (N = 4 for each group). D, *Ucp1* expression in brown preadipocytes treated with FGF8b for 48 h (N = 6 for each group). E, *Ucp1* expression in white inguinal preadipocytes treated with FGF8b for 48 h (N = 5 for each group). F, *Ucp1* expression in primary brown and white inguinal preadipocytes (stromal vascular fraction, SVF) treated with 125 ng/mL FGF8b for 48 h (N = 5 for each group). G, *Ucp1* expression in a time-course experiment over 96 h after single application of FGF8b in brown preadipocytes (N = 3 for control & 250-FGF8b groups, N = 5 for 125-FGF8b group). H, *Ucp1* expression in a dose-response experiment with varying concentrations of heparin (0.01-100 μg/) and FGF8b (0.2-125 ng/mL) in brown preadipocytes (N = 5 for each group). I, *Ucp1* expression in brown preadipocytes treated with equimolar (5.55 nM) concentrations of FGF1, FGF6, FGF8b, FGF9 and FGF21 (N = 5 for each group). J, *Ucp1* expression in brown preadipocytes treated with varying concentrations of FGF1 (N = 3 for each group). K, effect of a single dose of 125 ng/mL FGF8b on proliferation of brown preadipocytes (N = 3-4 for each group). L, Effect of passage number on FGF8b-mediated *Ucp1* expression in brown preadipocytes (N = 4 for each group). Data presented as means ± SD. FGF8b treated cells were co-treated with 1 μg/mL heparin in all experiments. Kruskal-Wallis test in (A, D, E, I, J). Mann-Whitney in (B), two-way ANOVA in (C, F, G, H, K, L). *$P < .05$, **$P < .01$, ***$P < .001$, ****$P < .0001$

dose-dependently increased *Ucp1* expression (Figure 1D,E) with an EC_{50} of approx. 55 ng/mL in brown preadipocytes (Figure S1A). Similarly, FGF8b treatment of primary preadipocytes (stromal-vascular fraction) isolated from the interscapular brown or inguinal white fat depot increased *Ucp1* expression by 25 and 40-fold, respectively (Figure 1F). A single application of FGF8b was examined over a 96 hours time course. Treatment with FGF8b resulted in a significant induction of *Ucp1* expression in brown preadipocytes within 48 hours, peaking at around 72 hours before declining again (Figure 1G). Subsequently, the ability of the cofactor heparin to modulate FGF8b signaling activity was determined in a dose-response experiment. Heparin concentrations in the range between 0.01 and 1 μg/mL amplified the effect of FGF8 on *Ucp1* expression by 2 to 6-fold (Figure 1H). Higher concentrations of heparin either blunted (10 μg/mL) or abrogated (100 μg/mL) the effect of FGF8b on *Ucp1* expression, highlighting the important role of heparin in modulating the bioavailability and signaling activity of paracrine FGF8b.

We then compared FGF8b to other paracrine (FGF1, FGF6, FGF9) and endocrine (FGF21) members of the FGF superfamily with respect to their capacity to induce *Ucp1* expression in cultured preadipocytes. The paracrine fibroblast growth factors FGF6 and FGF9 were included as they have been recently shown to regulate *Ucp1* expression in preadipocytes.[20] We observed that, when equimolar concentrations were used, all paracrine fibroblast growth factors, except FGF1, significantly increased *Ucp1* gene expression (Figure 1I). Higher concentrations of FGF1 eventually increased *Ucp1* expression, but remained less potent than FGF6, FGF8b and FGF9 (Figure 1J). The endocrine fibroblast growth factor FGF21 did not increase preadipocyte *Ucp1* expression in the presence of its cofactor beta Klotho (1 μg/mL), despite being a known inducer of *Ucp1* expression in mature adipocytes and adipose tissue.[12,13]

Fibroblast growth factors are known for their proliferative effect. We investigated a possible relationship between the mitogenic effect of FGF8b and *Ucp1* expression. Stimulation

of brown preadipocytes with FGF8b revealed a strong proliferative effect (Figure 1K). Other mitogens, however, such as epidermal growth factor (EGF) and platelet-derived growth factor (PDGF) failed to significantly increase *Ucp1* gene expression in brown preadipocytes (Figure S1B). Interestingly, we found that *Ucp1* induction by FGF8b increased in immortalized brown preadipocytes with higher passage numbers (Figure 1L), which indicates the existence of a highly proliferative and FGF8b-responsive subpopulation in the stromal-vascular fraction of brown adipose tissue. Importantly, while we identified FGF8b as a positive regulator of *Ucp1* in the undifferentiated preadipocyte, a negative impact on *Ucp1* expression was observed in differentiating and fully differentiated adipocytes, possibly due to its anti-adipogenic action (Figure S2A-C).

In summary, paracrine FGF8b strongly induced *Ucp1* expression in brown and white undifferentiated preadipocytes, a biological effect exhibited by all paracrine FGFs tested (FGF1, FGF6, FGF8b, FGF9), albeit to different degrees. Notably, the ability to induce *Ucp1* expression was amplified in preadipocytes of higher passage numbers and was not retained in differentiated adipocytes, suggesting that paracrine FGFs act specifically on highly proliferative, undifferentiated preadipocytes.

3.2 | FGF8b mediated *Ucp1* upregulation acts via a FGFR1-MEK-ERK signaling axis and controls glucose metabolism and ECM remodeling

We analyzed the transcriptome of white and brown preadipocytes to assess global changes in gene expression signatures upon FGF8b treatment (Figure 2A). We observed a remarkable overlap of both FGF8b up-and downregulated genes between preadipocytes of the two fat depots, demonstrating the effect of FGF8b to be essentially the same in both depots (Figure 2B). The 50 most responsive genes included
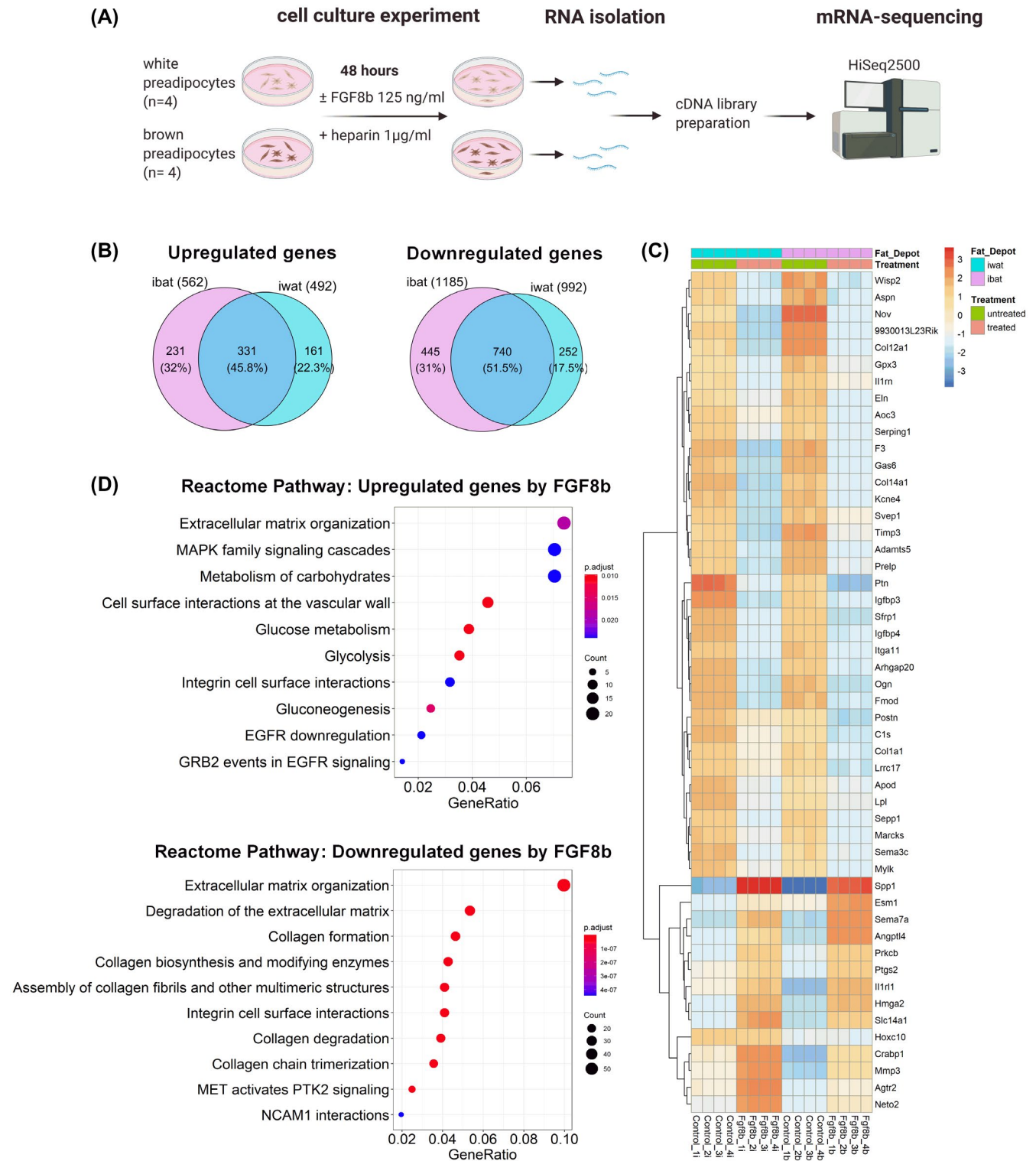
FIGURE 2 Transcriptomic analysis of FGF8b treatment of brown and white preadipocytes. A, RNA-Seq. experiment was performed on brown and white preadipocytes (*Ucp1*-reporter; N = 4 for each group; passage n° < 5) treated with 125 ng/mL FGF8b + 1 μg/mL heparin, control group was treated with 1 μg/mL heparin. B, Venn diagramms show the overlap between significantly up-and downregulated genes (adj. *P*-value <.01 and log2 fold change >1 or <−1) between fat depots (ibat vs. iwat). C, Heatmap of a subset of genes with the highest variance across all groups based on the variance stabilized transformed count matrix. Color scale reflects fold changes after variance stabilizing transformation (corresponds roughly to log2 fold changes) and are centered around the mean. D, Reactome pathway enrichment analysis of significantly up-and downregulated genes (adj. *P*-value <.01 and log2 fold change >1 or < −1)

downregulated genes such as *Ptn*, *Igfbp3*, *Igfbp4*, *Nov*, *Wisp2* and *Aspn* and upregulated genes such as *Spp1*, *Angptl4*, *Slc14a1*, *Hmga2* and *Ptgs2* (Figure 2C). Interestingly, *Ptgs2* (or cyclooxygenase-2) is an enzyme involved in the metabolism of arachidonic acid, a metabolic pathway which has been demonstrated to control recruitment of brown adipocytes in white adipose tissue before.[35,36] A pathway based enrichment analysis for downregulated genes identified *Extracellular matrix organization*, *Degradation of the extracellular matrix*, *Collagen formation* and *Collagen biosynthesis and modifying enzymes* as over-represented terms, indicating extracellular matrix (ECM) remodeling upon FGF8b treatment (Figure 2D). Significantly over-represented terms for upregulated genes included *Extracellular matrix organization*, *MAPK family signaling cascade*, *Metabolism of carbohydrates*, *Glucose metabolism* and *Glycolysis*, highlighting the role of FGF8b in regulating glucose utilization, possibly by activation of the MAPK pathway. We subsequently focused on three key findings and examined them

more extensively. Firstly, does FGF8b act via the MAPK pathway or do other FGF signaling branches contribute to the induction of *Ucp1*? Secondly, is the strong induction of *Ptgs2* (*Cox2*) gene expression embedded in a broader upregulation of prostaglandin metabolism with potential impact on *Ucp1* gene expression? And lastly, is the induction of glycolytic gene expression upon FGF8b treatment linked to the transcriptional regulation of *Ucp1* or secondary to it?

We probed the entire FGF signaling cascade, from the receptor level to several branching signaling pathways to decipher the functional dependencies underlying the FGF8b effect. We used dicer-substrate short interfering RNAs (dsiR-NAs) to silence *Fgfr1* and *Fgfr2*, the most abundant FGF-receptors in preadipocytes (Figure 3A). Knockdown of *Fgfr1* significantly increased *Fgfr2* transcript levels, whereas knockdown of *Fgfr2* did not affect *Fgfr1* transcript levels (Figure 3B,C). Treatment with FGF8b completely lost its effect on *Ucp1* expression only in brown preadipocytes lacking *Fgfr1*, but not *Fgfr2* (Figure 3D). Knockdown efficiency of
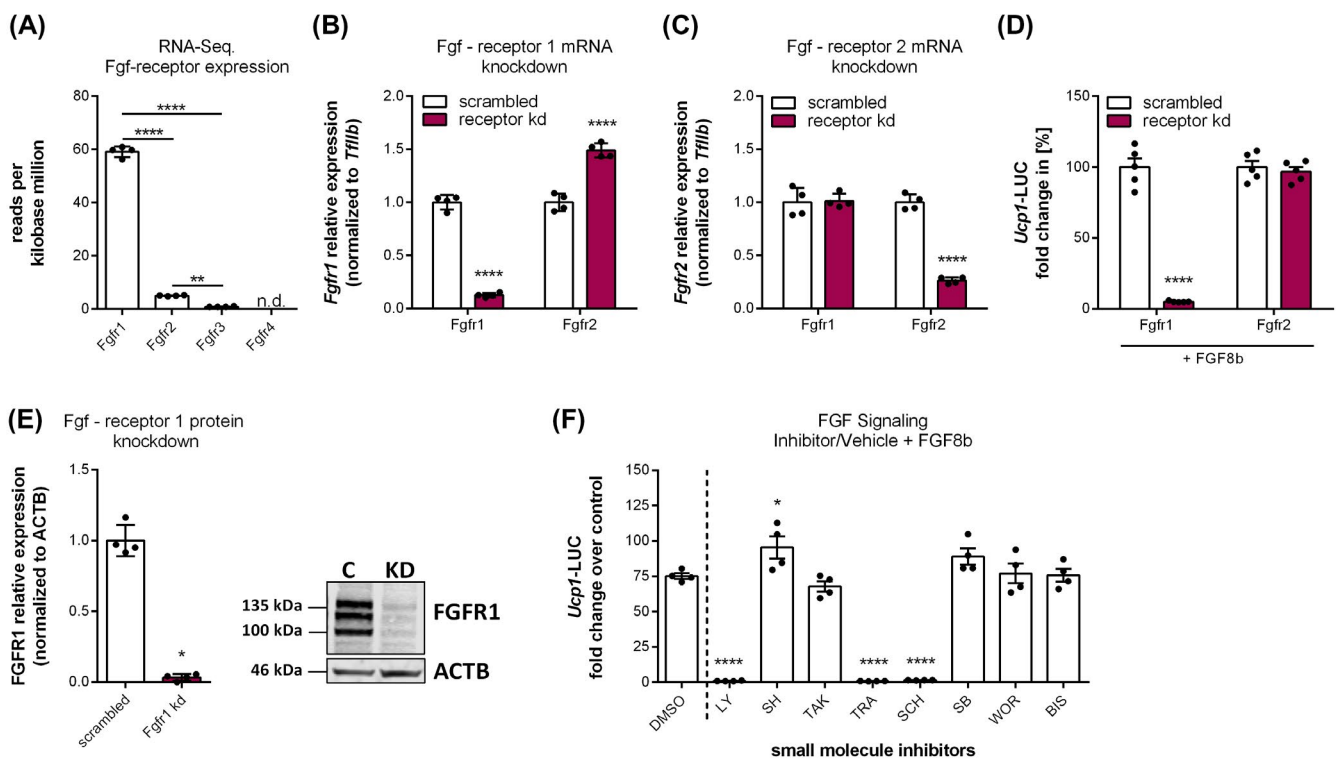

FIGURE 3 FGF8b mediated upregulation of *Ucp1* signals via a FGFR1-MEK1/2-ERK1/2 axis. A, *Fgfr* mRNA expression in RNA-Seq. experiment in reads per million mapped reads (RPKM) in brown preadipocytes (N = 4 for each group). B and C, *Fgfr1/Fgfr2* mRNA expression 48 h post-transfection in *Fgfr1/Fgfr2* knockdown (kd) experiments with 20 nM dsiRNA in brown preadipocytes (N = 4 for each group). D, effect of *Fgfr1/Fgfr2* knockdown (kd) on *Ucp1* expression in brown preadipocytes treated with 125 ng/mL FGF8b for 48 h (N = 5 for each group). E, FGFR1 protein expression 72 h post-transfection in *Fgfr1* knockdown experiment with 20 nM dsiRNA in brown preadipocytes. Data normalized to ACTB protein expression (N = 4 for each group; C = Control, KD =FGFR1 knockdown). F, Fold change in *Ucp1* expression in brown preadipoctes co-treated for 48 h with 125 ng/mL FGF8b and 250 nM of the following inhibitors (abbreviation, target): LY2874455 (LY, pan-FGFR), SH-4-54 (SH, Stat3,5), TAK632(TAK, pan-RAF), Trametinib (TRA, MEK1/2), SCH772984(SCH, ERK1/2),SB2020190 (SB, p38MAPK), Wortmannin (WOR, PI3K), Bisindoylmaleimide I (BIS, PKC) (N = 4 for each group). Data presented as means ± SD. FGF8b treated cells were co-treated with 1 µg/mL heparin in all experiments. One-way ANOVA in (A and F), two-way ANOVA (B-D), Mann-Whitney test in (E). *$P < .05$, **$P < .01$, ***$P < .001$, ****$P < .0001$

FGFR1 expression was validated on protein level (Figure 3E). Thus, FGFR1 mediated FGF8b-induced *Ucp1* expression in preadipocytes.

A panel of seven small molecule inhibitors was employed to target four different pathways including Ras-MAPK, PI3K-AKT, STAT3,5 and PLCγ-PKC (Table 1). The efficacy of each inhibitor to abrogate the *Ucp1* inducing effect of FGF8b was assessed and compared to a vehicle control and the pan-FGFR inhibitor LY2874455, which inhibits FGF-receptor auto-phosphorylation. *Ucp1* expression increased by 75-fold in the control group and was completely abrogated by FGFR inactivation (Figure 3F). Four of the seven inhibitors did not affect FGF signaling (TAK632, SB2020190, Wortmannin, Bisindoylmaleimide I), one enhanced FGF signaling (SH-4-54) by 25% and two abolished the effect entirely (Trametinib, SCH772984) (Figure 3F). Taken together, receptor knockdown studies and probing of all relevant signaling branches of the FGF signaling pathway revealed that FGF8b induced *Ucp1* expression via a FGFR1-MEK1/2-ERK1/2 axis of the MAPK pathway (Figure 4).

The nuclear receptors Peroxisome proliferator-activated receptors (PPARs) are known to regulate transcription of the *Ucp1* gene during brown adipocyte differentiation. We therefore tested whether PPARs are downstream effectors of the FGF8b activated FGFR1-MEK1/2-ERK1/2 signaling cascade controlling *Ucp1* expression. Surprisingly, PPARs were not involved downstream of the FGF8b signaling cascade to control *Ucp1* expression (Figure S3A), suggesting non-classical transcriptional regulators to be involved.

3.3 | FGF8b regulates prostaglandin metabolism and PGE$_2$ production to upregulate *Ucp1* expression

We investigated the impact of FGF8b on prostaglandin metabolism as suggested by our transcriptomic analysis. Indeed, most genes along the entire arachidonic acid pathway were upregulated after 48 hours of FGF8b treatment. These genes included *Pla2g4a*, *Ptgs1* (*Cox1*), *Ptgs2* (*Cox2*), *Ptges1*

and *Slco2a1 and* were validated by RT-qPCR (Figure 5A). Moreover, inhibition of *Ptgs1* and *Ptgs2* by non-selective COX inhibitors diclofenac and indomethacin significantly reduced, while selective COX2 inhibitor celecoxib completely abrogated the effect of FGF8b on *Ucp1* expression (Figure 5B). Having established that FGF8b affects *Ucp1* expression in a COX2-dependent manner, we moved downstream of the pathway to identify potential candidate compounds that causally link prostaglandin metabolism with *Ucp1* expression. To this end, we quantified 52 oxylipins in cell culture supernatant of brown preadipocytes treated with either FGF8b, celecoxib or a combination of both. From the entire panel of 52 oxylipins 6 were robustly detectable in FGF8b conditioned media and passed internal quality control (Figure 5C). Two prostaglandins, PGE$_2$ and 6-keto-PGF$_{1\alpha}$, a degradation product of PGI$_2$, were identified as potential candidates as they constituted the two most abundant oxylipins detected, were both increased by FGF8b and decreased when preadipocytes were treated with the Cox2 inhibitor celecoxib (Figure 5D). We first addressed the question whether PGE$_2$ biosynthesis was necessary for FGF8b mediated *Ucp1* expression. To this end, we co-stimulated brown preadipocytes with FGF8b and inhibitors of the PGE$_2$ producing enzyme PTGES1 (CAY10678, CAY10526). Both PTGES1 inhibitors strongly blunted the upregulation of *Ucp1* by FGF8b when applied individually and more effectively when given in combination (Figure 5E). In contrast, inhibition of the PGI$_2$ synthesizing enzyme PTGIS by U-51605 did not affect *Ucp1* upregulation by FGF8b, despite robustly reducing its stable metabolite 6-keto-PGF$_{1\alpha}$ (Figure S4A,B). Additionally, knockdown of *Ptges1* significantly reduced *Ucp1* expression upon FGF8b treatment with a concomitant decrease in PGE$_2$ levels in cell media (Figure 5F-H). To confirm that PGE$_2$ production in response to FGF8b precedes the induction of *Ucp1* gene expression, a time-course experiment over 48 hours was performed. Levels of PGE$_2$ in cell media rapidly increased within hours of treatment and peaked after 24 hours (Figure 5I), while *Ucp1* induction followed with a delay of at least 24 hours, establishing a clear sequence of events (Figure 5J). Thus,

TABLE 1 Small molecule inhibitors targeting the FGF signaling pathway

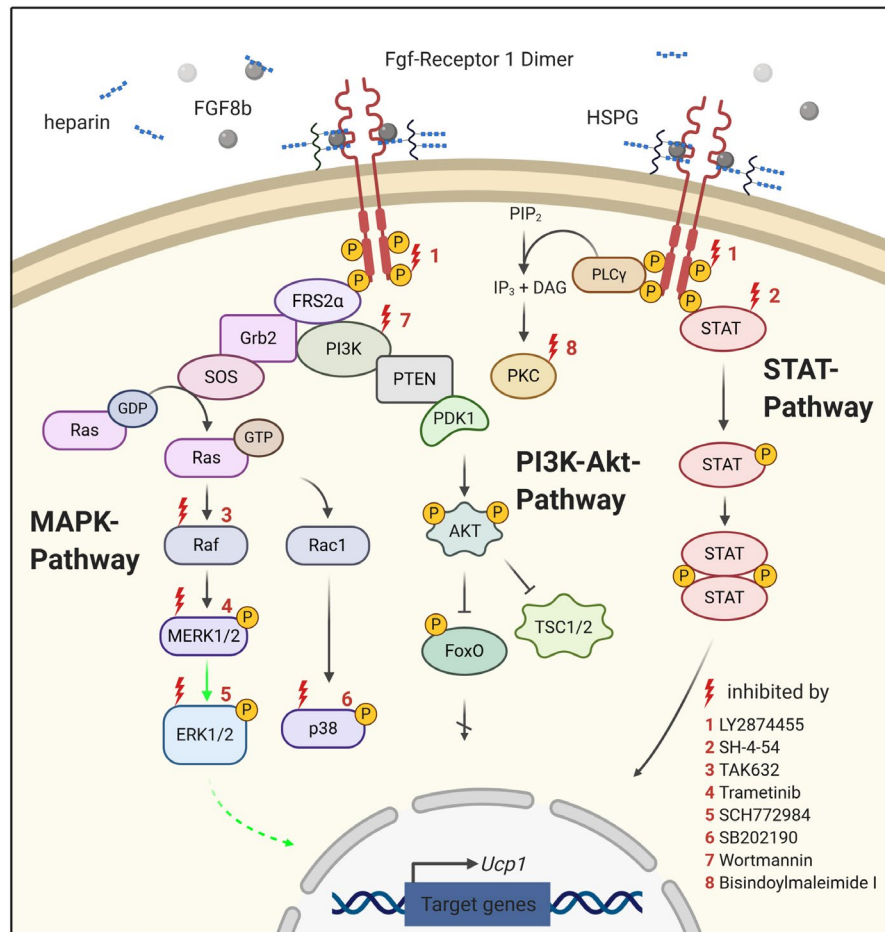| No.	Inhibitor name	Abbreviation	Target	Pathway
1	LY2874455	LY	pan-FGFR	-
2	SH-4-54	SH	Stat3,5	STAT
3	TAK632	TAK	pan-RAF	RAS-MAPK
4	Trametinib	TRA	MEK1/2	RAS-MAPK
5	SCH772984	SCH	ERK1/2	RAS-MAPK
6	SB202190	SB	p38MAPK	RAS-MAPK
7	Wortmannin	WOR	PI3K	PI3K-AKT
8	Bisindoylmaleimide I	BIS	PKC	PLCγ-PKC

FIGURE 4 Fibroblast growth factor signaling pathway. The signaling cascade is initiated by formation of the ternary FGF8b-heparin/heparan sulfate proteoglycans (HSPG)-FGFR1 complex, which results in receptor dimerization and receptor tyrosine kinase driven autophosphorylation. Four main intraceullular signaling pathways are consequently activated including the MAPK, PI3K-Akt, STAT and PLCγ-PKC pathways. A panel of eight small molecule inhibitors were used to target these individual signaling pathways in order to delineate the contribution of each to FGF8b induced *Ucp1* expression. The following inhibitors (abbreviation + target) were used: (1) LY2874455 (LY, pan-FGFR), (2) SH-4-54 (SH, Stat3,5), (3) TAK632(TAK, pan-RAF), (4) Trametinib (TRA, MEK1/2), (5) SCH772984(SCH, ERK1/2), (6) SB2020190(SB, p38MAPK), (7) Wortmannin (WOR, PI3K), (8) Bisindoylmaleimide I (BIS, PKC). A green solid arrow indicates the experimentally established contribution of the FGFR1-MEK1/2-ERK1/2 axis. Figure created with biorender.com

PGE$_2$ production was shown to be a necessary component of FGF8b mediated *Ucp1* expression. To investigate whether PGE$_2$ was sufficient to increase *Ucp1* expression in cultured cells, we incubated brown preadipocytes with 10 and 100 μM of PGE$_2$ for 8 and 48 hours. We found that 8 hours of incubation with high micromolar concentrations of PGE$_2$ upregulated *Ucp1* expression up to 8-fold, whereas 48 hours of incubation did not have an effect (Figure 5K). In summary, FGF8b coordinately upregulated genes within the prostaglandin biosynthetic pathway to control *Ucp1* expression in a COX2 and PTGES1-dependent manner and PGE$_2$, the product of the enzymatic action of PTGES1, is an abundant FGF8b-responsive metabolite with the ability to rapidly and transiently induce *Ucp1* in undifferentiated preadipocytes. Thus, we established a mechanism of FGF8b mediated *Ucp1* expression involving the sequential action of COX2, PTGES1 and PGE$_2$.

3.4 | Increased glycolytic flux is required for full upregulation of *Ucp1* gene expression

Our pathway enrichment analysis suggested that FGF8b treatment positively regulates glucose catabolism. We therefore examined whether FGF8b treatment promotes glycolysis in preadipocytes. Analysis of our transcriptomic data confirmed that most glycolytic genes, including *Slc2a1*, *Hk2*, and *Ldha*, were significantly upregulated in response to FGF8b (Figure 6A). On the functional level, preadipocytes became more glycolytic, more metabolically active and increased proton production rate dose-dependently upon FGF8b treatment (Figure 6B-D). One factor potentially contributing to increased glycolytic flux is enhanced glucose uptake. We observed that FGF8b treatment resulted in a 6-fold increase in the uptake rate of glucose, which was completely abolished when cells
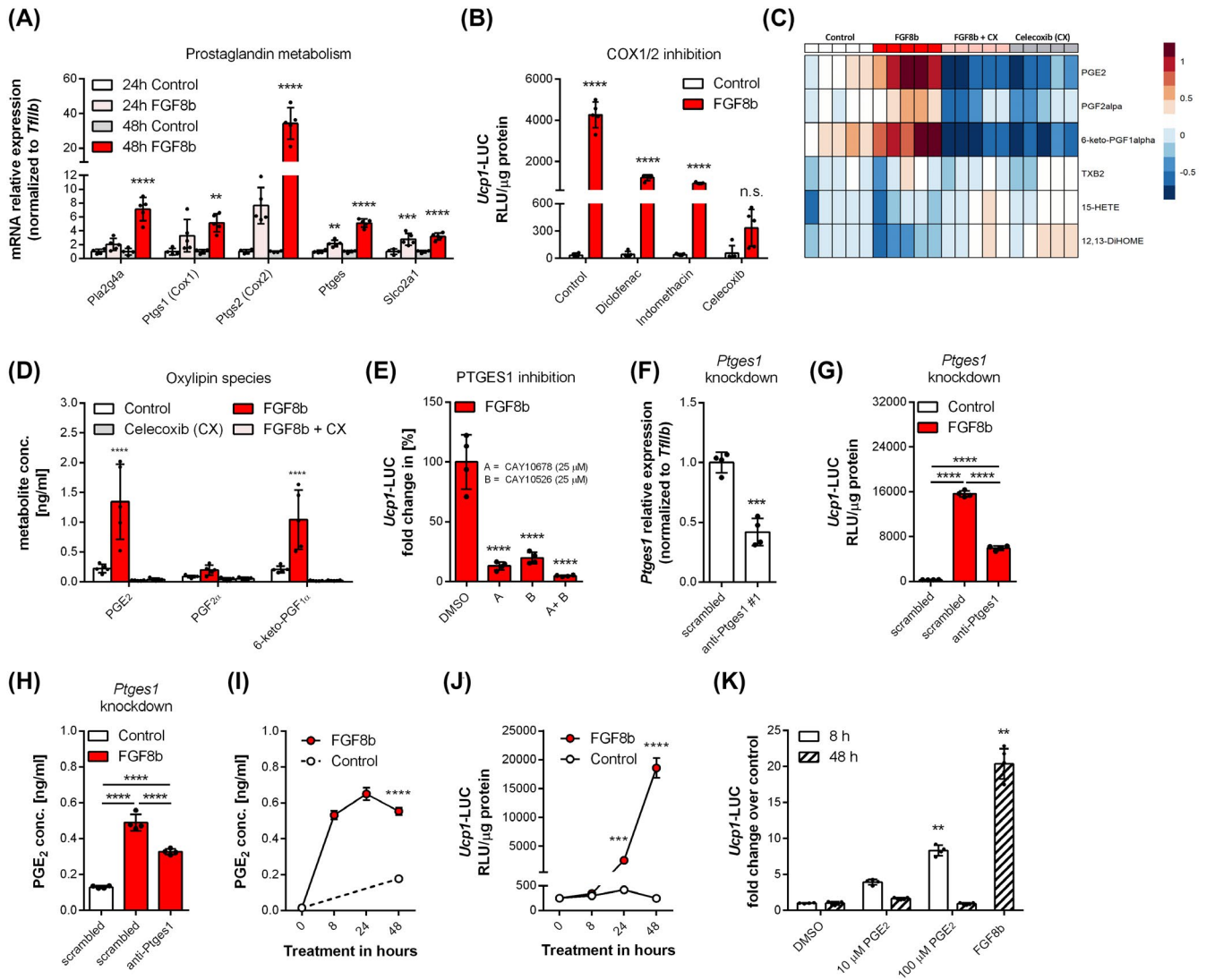
FIGURE 5 FGF8b regulates prostaglandin metabolism and PGE2 production to upregulate *Ucp1* expression. A, mRNA expression of genes involved in prostaglandin metabolism in brown preadipocytes treated with 125 ng/mL FGF8b for 24 and 48 h (N = 4 for each group). B, Cyclooxygenase (COX) inhibition by unselective COX1/2-inhibitor diclofenac (20 μM) and indomethacin (125 μM) and selective COX2 inhibitor celecoxib (20 μM) in brown preadipocytes treated with 125 ng/mL FGF8b for 48 h (N = 5 for each group). C and D, Oxylipin measurements by LC-MS/MS in conditioned media of brown preadipocytes treated with combinations of 125 ng/mL FGF8b and/or 20 μM celecoxib (CX) for 48 h. Scale in (C) centered around the mean represents log10 transformed metabolite concentrations in pg/mL (N = 5 for each group). E, inhibition of PTGES1 by CAY10678 and/or CAY10526 in brown preadipocytes treated with 125 ng/mL FGF8b for 48 h (N = 4 for each group). F, *Ptges1* mRNA expression 48 h post-transfection in *Ptges1* knockdown experiment with 20 nM dsiRNA in brown preadipocytes (N = 4 for each group). G, effect of *Ptges1* knockdown on *Ucp1* expression in brown preadipocytes treated with 125 ng/mL FGF8b for 48 h (N = 4 for each group). H, effect of *Ptges1* knockdown on PGE2 levels in brown preadipocytes treated with 125 ng/mL FGF8b for 48 h (N = 4 for each group). I, induction of PGE2 in cell media and (J) *Ucp1* expression upon 125 ng/mL FGF8b treatment after 8, 24 and 48 h in brown preadipocytes (N = 4 for each group). K, Incubation of brown preadipocytes with 10 and 100 μM Prostaglandin E2 for 8 h and 48 h. Fgf8b treatment for 48 h (N = 4 for 8 h treatment groups; N = 5 for 48 h treatment groups). Data presented as means ± SD. FGF8b treated cells were co-treated with 1 μg/mL heparin in all experiments. Two-way ANOVA in (A, B, D, J), one way-ANOVA in (E, G, H), Kruskal-Wallis in (K) for each treatment duration and Student's *t*-test in (F) and (I) (for timepoint 48 h only).*$P < .05$, **$P < .01$, ***$P < .001$, ****$P < .0001$

were co-incubated with 10 μM of the glucose transporter 1 inhibitor BAY-876 (Figure 6E). Since one hallmark of glycolytic cells is lactate production, accumulation of lactate in the media was monitored over a 96 hours time span following a single application of FGF8b. Lactate levels dramatically increased from <0.35 mM at the beginning

to >5 mM after 96 hours in the FGF8b group, whereas cell culture media of untreated cells only accumulated 2 mM lactate in the same time period (Figure 6F). Importantly, glycolytic and mitochondrial gene expression data (Figure S5A,B) and lactate accumulation upon FGF8b treatment (Figure 6G) was shown not to depend on the presence of
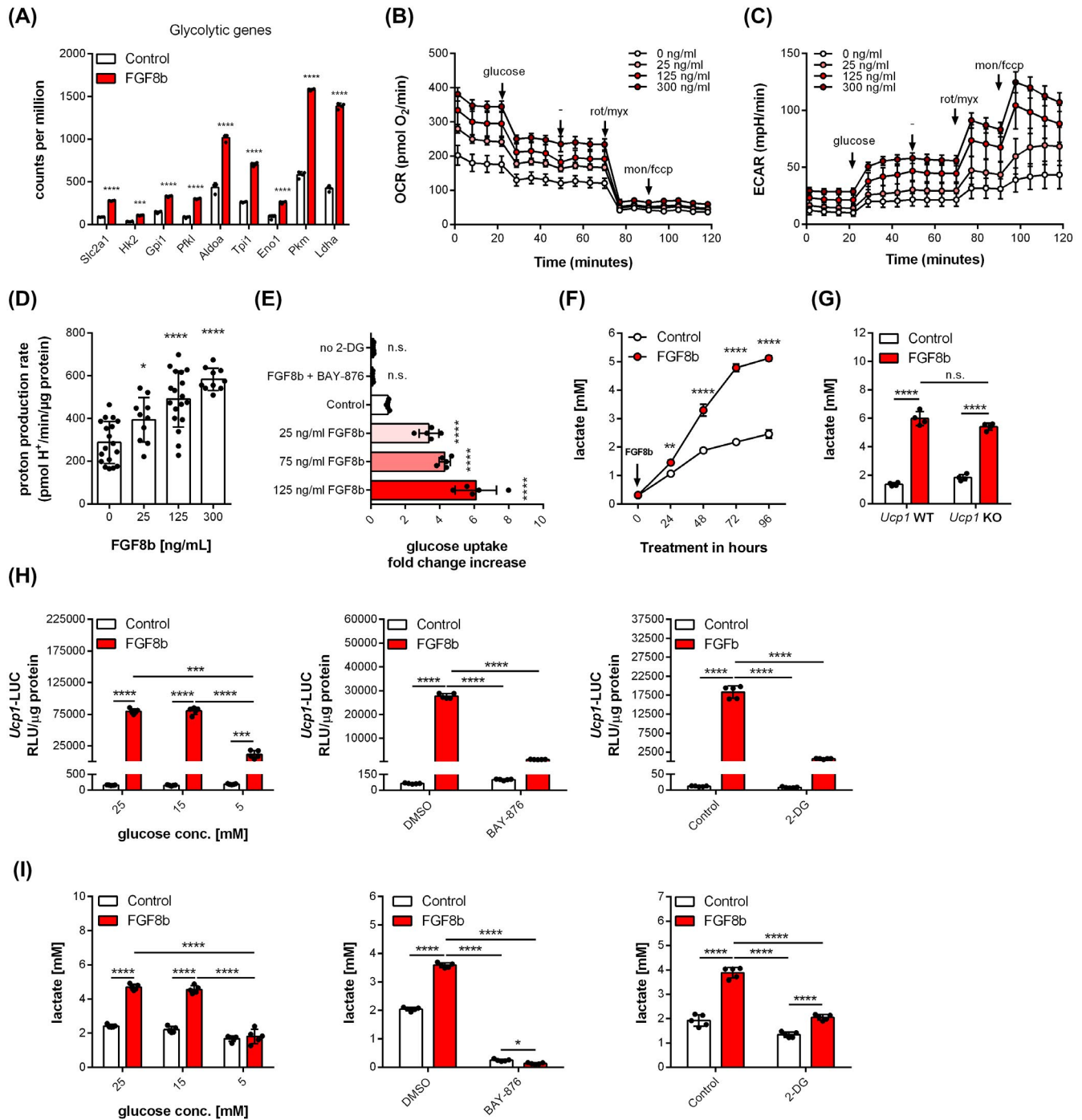
FIGURE 6 Increased glycolytic flux is required for full upregulation of *Ucp1* gene expression. A, Gene expression of glycolytic genes from RNA-Seq. Experiment in counts per million in brown preadipocytes upon treatment with 125 ng/mL FGF8b for 48 h (N = 4 for each group). B, Oxygen consumption rate (OCR) and (C) extracellular acidification rate (ECAR) measured in FGF8b treated (48 h) brown preadipocytes on a Seahorse XF96 Extracellular Flux Analyzer. Data presented as means ±SEM (n = 18 for control & 125-FGF8b groups, n = 10 for 25-FGF8b & 300-FGF8b groups). D, Glycolytic proton production rate (PPRglyc) calculated from OCR and ECAR in brown preadipocytes treated with FGF8b. E, fold change in glucose uptake capacity in brown preadipocytes (129S6Sv/Ev Tac) treated with FGF8b and 10 μM of the SLC2A1 (GLUT1) inhibitor BAY-876 for 48 h (N = 5 for each group). F, Lactate accumulation in cell media over time after application of a single dose of 125 ng/mL FGF8b in brown preadipocytes (N = 3 for each group). G, Lactate levels in cell media in FGF8b (125 ng/mL) treated (48 h) brown preadipocytes (WT-129S vs Ucp1-KO) (N = 4 for each group). H, *Ucp1* expression in FGF8b treated (48 h) brown preadipocytes depending on (1) varying glucose levels in the cell media, (2) glucose uptake inhibition by 2 μM BAY-876, (3) inhibition of glycolysis by 2.5 mM 2-deoxyglucose (2-DG) (N = 5 for each group). I, Lactate levels in cell culture media in experiments described in panel h. Data presented as means ± SD. FGF8b treated cells were co-treated with 1 μg/mL heparin in all experiments. Multiple Student's *t*-test in (A), one-way ANOVA in (D and E), two-way ANOVA in (F-I). $*P < .05$, $**P < .01$, $***P < .001$, $****P < .0001$

Ucp1. Thus, glycolysis impacts *Ucp1* expression, but the induction of *Ucp1* is not linked to the emergence of the glycolytic phenotype upon FGF8b treatment.

We next sought to manipulate the rate of glycolytic flux and examine the effect on FGF8b-mediated *Ucp1* expression. In order to achieve reduced glycolytic flux three different approaches were employed: (1) glucose levels in cell culture media were reduced, (2) glucose uptake was inhibited by non-toxic concentrations of BAY-876 and (3) glycolysis was inhibited by 2.5 mM 2-deoxy-glucose (2-DG). In each of these experiments, FGF8b-mediated *Ucp1* expression was significantly reduced (Figure 6H), while lower lactate levels in the intervention groups validated the experimental design (Figure 6I). Thus, we demonstrated that FGF8b regulates glucose metabolism by strongly promoting glucose uptake and glycolysis. Pharmacological manipulation of glucose metabolism revealed that FGF8b induced high glycolytic flux is a requirement for FGF8b mediated *Ucp1* expression.

Notably, pharmacological inhibition of the FGFR1-MEK1/2-ERK1/2 signaling axis, described above, abolished the FGF8b driven lactate release completely (Figure S3D). Since lactate is able to control *Ucp1* expression in white adipocytes,[37] we hypothesized that lactate may mediate FGF8b induced *Ucp1* expression. Indeed, when additional lactate was added to FGF8b containing cell culture media, *Ucp1* expression was dose-dependently increased up to 50 mM additional lactate (Figure 7A), while lactate alone did not have any effect (Figure 7B). To test whether lactate production was required for FGF8b mediated *Ucp1* expression, we pharmacologically inhibited lactate production with the competitive LDHA inhibitor sodium oxamate. Despite effectively reducing lactate production (Figure 7C), FGF8b mediated *Ucp1* expression remained unaffected by LDHA inhibition (Figure 7D). These data indicated that even though additional lactate positively contributed to *Ucp1* expression upon FGF8b treatment, lactate production per se was not required for the upregulation of *Ucp1* by FGF8b. In summary, high glycolytic flux, not its product lactate, is necessary but not sufficient to induce *Ucp1* expression upon FGF8b treatment.
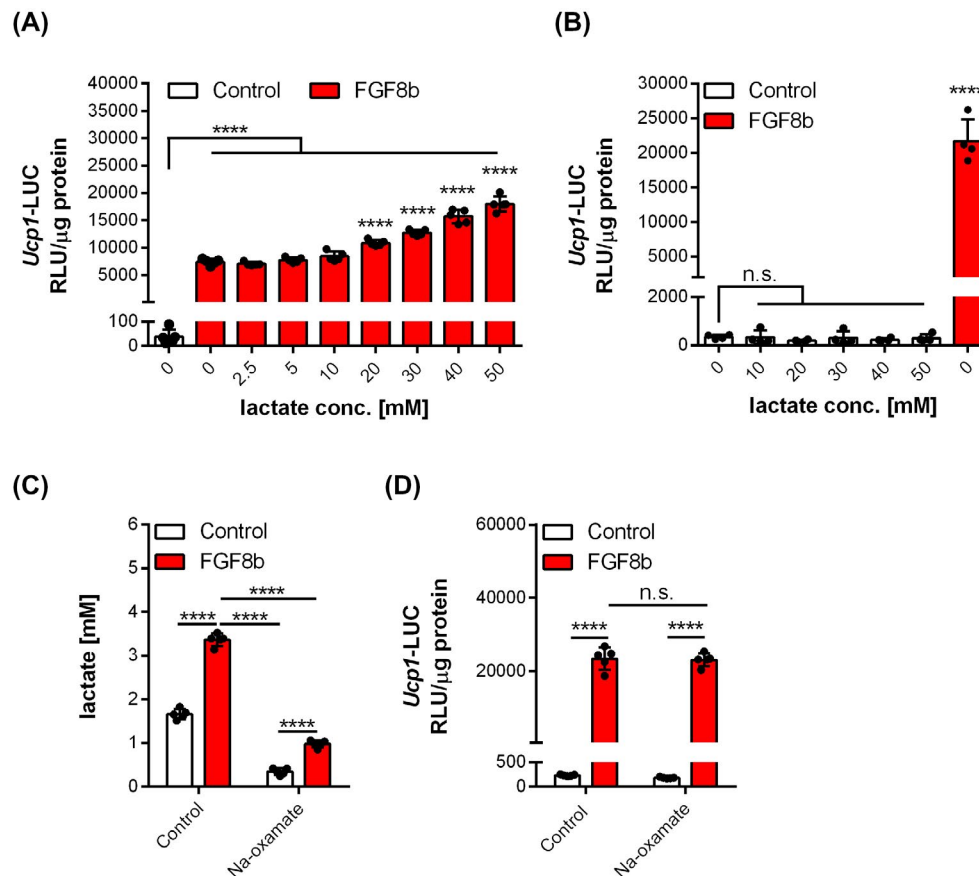

FIGURE 7 Lactate contributes to FGF8b mediated *Ucp1* expression, but is not required. A, Brown preadipocytes co-treated with 125 ng/mL FGF8b and varying concentrations of lactate (2.5-50 mM) for 48 h (N = 4 for each group). B, Brown preadipocytes treated with 125 ng/mL FGF8b or varying concentrations of lactate (10-50 mM) for 48 h (N = 4 for each group). C, Effect of sodium oxamate treatment (20 mM) of brown preadipocytes for 48 h on lactate levels in cell culture media and (D) FGF8b mediated *Ucp1* expression (N = 5 for each group). Data presented as means ± SD. FGF8b treated cells were co-treated with 1 μg/mL heparin in all experiments. One-way ANOVA in (A and B) two-way ANOVA in (C and D). *$P < .05$, **$P < .01$, ***$P < .001$, ****$P < .0001$

3.5 | FGF1 does not promote high glycolytic flux, thus fails to fully induce *Ucp1* expression despite intact PGE₂ production

Interestingly, slowing down glycolytic flux by inhibiting glucose uptake with BAY-876 did not abolish FGF8b-mediated PGE₂ production (Figure 8A). On the contrary, expression of prostaglandin metabolism related genes was induced when glucose uptake was inhibited (Figure 8B), highlighting that prostaglandin and glucose metabolism interact with each other and that PGE₂ production alone is not sufficient to fully activate *Ucp1* transcription in the absence of high glycolytic flux. Revisiting that from all tested paracrine FGFs, FGF1 was the least effective in inducing *Ucp1* expression,

we hypothesized that FGF1 fails to activate either PGE₂ synthesis, glycolytic flux or both. Treatment of brown preadipocytes with equimolar concentrations of FGF8b and FGF1 showed that FGF1 was able to elevate PGE₂ in cell culture media to levels seen in the FGF8b group (Figure 8C) and that the induction of *Ptgs2* (*Cox2*) was intact (Figure 8D). However, when a glucose uptake assay was performed, it was evident that FGF1 failed to increase glucose uptake above control levels (Figure 8E), possibly due to lower efficacy in inducing gene expression of glycolytic genes (Figure 8F). Importantly, the effect of FGF1 on expression levels of glycolytic genes was dose-dependent, reminiscent of the dose-dependent effect of FGF1 on *Ucp1*, as shown earlier (Figure 1J). Additionally, when glucose consumption was
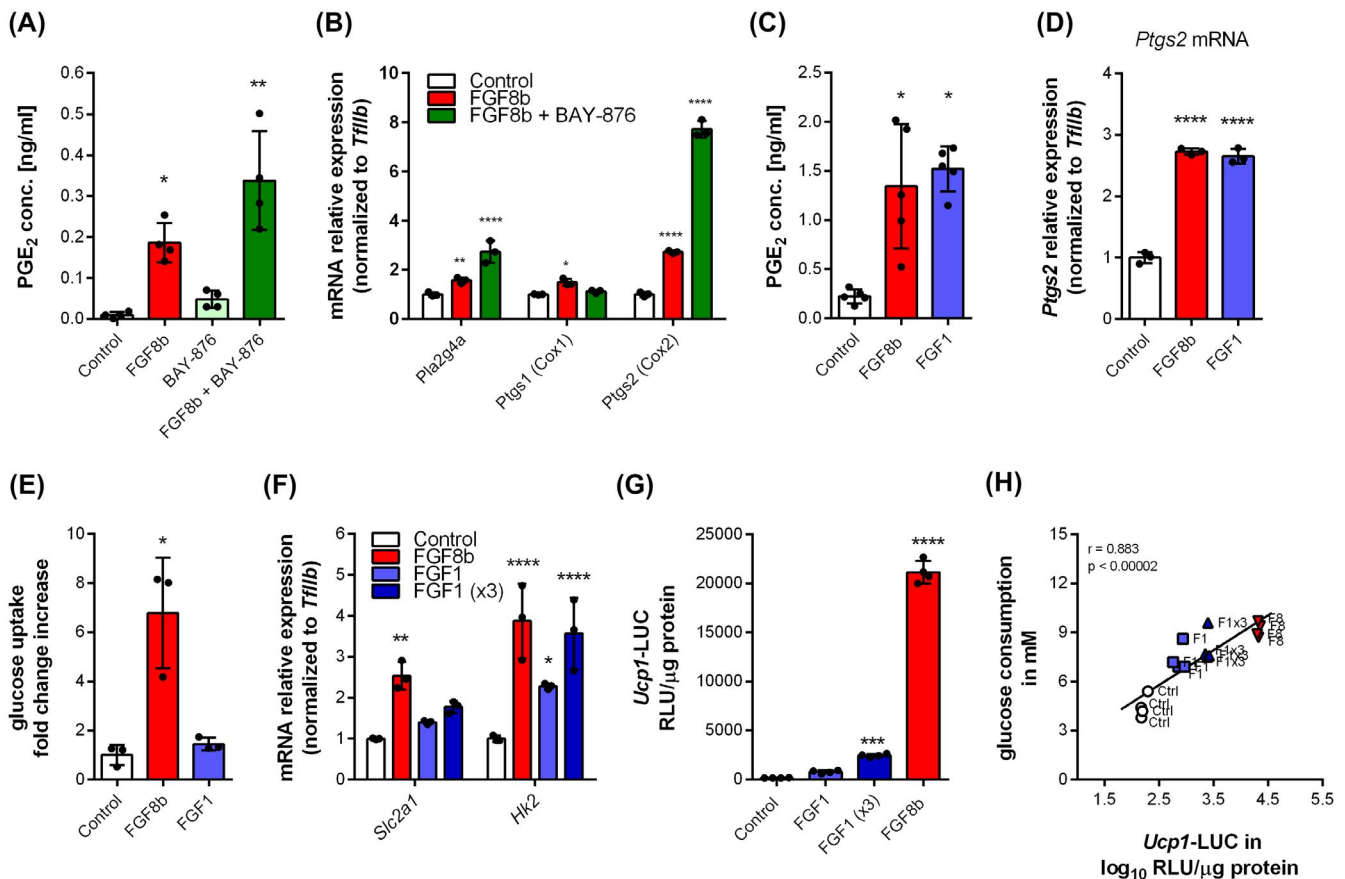

FIGURE 8 FGF1 does not promote high glycolytic flux, thus fails to induce *Ucp1* expression despite intact PGE₂ production. A, PGE₂ concentration in conditioned cell culture media of brown preadipocytes treated with combinations of FGF8b (125 ng/mL) and BAY-876 (2 μM) for 48 h (N = 4 for each group). B, mRNA expression of genes related to prostaglandin metabolism in brown preadipocytes (129S6Sv/Ev Tac) treated with combinations of FGF8b (125 ng/mL) and BAY-876 (2 μM) for 48 h (N = 3 for each group). C, PGE2 concentration in conditioned cell culture media of brown preadipocytes treated with equimolar concentrations (5.55 nM) of FGF1 and FGF8b for 48 h (N = 5 for each group). D, *Ptgs2* (*Cox2*) mRNA expression of brown preadipocytes treated with equimolar concentrations (5.55 nM) of FGF1 and FGF8b for 48 h (N = 3 for each group). E, glucose uptake in brown preadipocytes (129S6Sv/Ev Tac) treated with equimolar concentrations (5.55 nM) of FGF1 and FGF8b for 48 h (N = 3 for each group). F, mRNA expression of genes related to glucose metabolism in brown preadipocytes treated with FGF8b and FGF1 for 48 h (N = 3 for each group). G, effect of a 48 h treatment with FGF1 (5.55 nM), FGF1 (16.5 nM) and FGF8b (5.55 nM) on *Ucp1* expression in brown preadipocytes (N = 4 for each group). H, correlation between glucose consumption and *Ucp1* expression (plotted in g) in brown preadipocytes treated with either 5.55 nM FGF1, 16.5 nM FGF1 (= FGF1 x3) or 5.55 nM FGF8b (N = 4 for each group). Data presented as means ± SD. FGF8b treated cells were co-treated with 1 μg/mL heparin in all experiments. Kruskal-Wallis in (A, C and E), two-way ANOVA in (B and F), one-way ANOVA in (D and G). Spearman correlation in (H). *$P < .05$, **$P < .01$, ***$P < .001$, ****$P < .0001$

plotted against *Ucp1* transcription upon treatment with FGF1 and FGF8b (Figure 8G), a significant correlation (r = 0.883) was observed (Figure 8H). Taken together, we showed that paracrine FGFs co-regulate prostaglandin and glucose metabolism to control *Ucp1* expression and failure to co-activate either of the two metabolic pathways prevents a full-scale induction of *Ucp1*.

3.6 | The transcriptional regulators *Nrf1* and *Hes1* are required for FGF8b mediated *Ucp1* expression

Although we demonstrated prostaglandin and glucose metabolism to play key roles in regulating FGF8b mediated *Ucp1* expression, the underlying transcriptional regulators remained elusive. We therefore decided to perform a second transcriptomic analysis to correlate gene expression

signatures of potential transcriptional regulators with *Ucp1* expression upon treatment with three different paracrine FGFs: FGF1, FGF8b and FGF9. We also included a group to reflect impaired glycolytic flux, as a result of BAY-876 treatment, in the presence of FGF8b. We analyzed the principal components of the dataset and found that the FGF1 group showed closer proximity to the control group than to any other group (Figure 9A). Interestingly, the FGF8b and FGF9 groups clustered together indicating extremely high similarity in gene expression patterns, which resulted in a very high correlation coefficient of r = 0.999 when mapped FPKM distributions were compared (Figure S6). As expected, both FGF8b and FGF9 strongly upregulated *Ucp1*, whereas FGF1 failed to do so and FGF8b co-stimulated with BAY-876 only mildly increased *Ucp1* (Figure 9B). Since the gene expression signatures between FGF8b and FGF9 were virtually identical, we examined a recently discovered transcriptional complex, which has
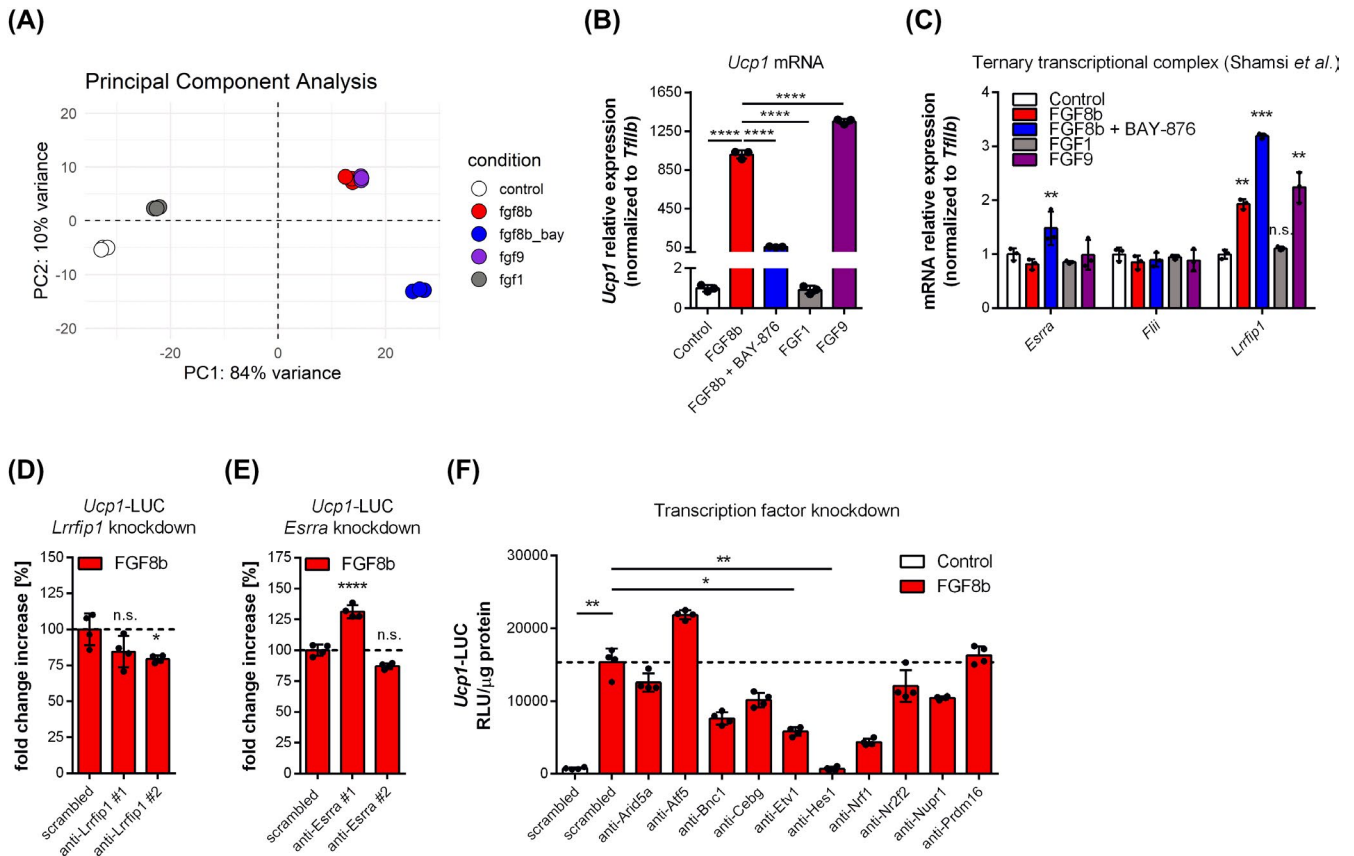

FIGURE 9 The transcriptional regulators *Nrf1* and *Hes1* are required for FGF8b mediated *Ucp1* expression. A, principal component analysis of gene expression patterns induced by treatment with equimolar concentrations (5.55 nM) of FGF1, FGF8b (± 2 µM BAY-876) and FGF9 for 48 h in brown preadipocytes (129S6Sv/Ev Tac) (N = 3 for each group). B, *Ucp1* mRNA expression induced by treatment with equimolar concentrations (5.55 nM) of FGF1, FGF8b (± 2 µM BAY-876) and FGF9 for 48 h in brown preadipocytes (129S6Sv/Ev Tac) (N = 3 for each group). C, mRNA expression of *Esrra*, *Flii*, *Lrrfip1* in brown preadipocytes treated with equimolar concentrations (5.55 nM) of FGF1, FGF8b (± 2 µM BAY-876) and FGF9 for 48 h (N = 3 for each group). D and E, *Ucp1* expression following knockdown of *Lrrfip1* and knockdown of *Esrra* in FGF8b treated brown preadipocytes (N = 4 for each group). E, Effect of knockdown of possible transcriptional regulators on FGF8b mediated *Ucp1* expression in brown preadipocytes (N = 4 for each group). Data presented as means ± SD. FGF8b treated cells were co-treated with 1 µg/mL heparin in all experiments. One-way ANOVA in (B, D, and E), two-way ANOVA in (C). *P < .05, **P < .01, ***P < .001, ****P < .0001

been causally linked to FGF9 mediated *Ucp1* expression in preadipocytes.[20] The three-component-complex consists of the estrogen-related receptor α (*Esrra*), flightless-1 (*Flii*) and leucine-rich-repeat-(in Flii)-interacting-protein-1 (*Lrrfip1*). Interestingly, treatment of brown preadipocytes with FGF8b and FGF9 induced transcript levels of the transcriptional co-activator *Lrrfip1* two-fold, while FGF1 treatment did not change *Lrrfip1* transcript levels (Figure 9C), which correlated with their capacity to induce *Ucp1*. We subsequently performed knockdown experiments of *Lrrfip1* and *Esrra*, both shown to be necessary and sufficient components for FGF9 mediated *Ucp1* induction.[20] FGF8b mediated *Ucp1* expression was, however, only marginally affected by *Lrrfip1* knockdown (Figure 9D), albeit significantly (in one of two employed dsiRNAs), whereas knockdown of *Esrra* did neither reduce FGF8b (Figure 9E) nor FGF9 induced *Ucp1* expression (Figure S4G). Thus, the reported transcription factors *Esrra* and *Lrrfip1* were not required for FGF8b and FGF9 mediated *Ucp1* expression in preadipocytes in our hands. We subsequently scanned the data set for genes with transcription factor binding activity that highly correlated with *Ucp1* gene expression across all groups. We extracted ten potential transcriptional regulators (*Arid5a*, *Atf5*, *Bnc1*, *Cebg*, *Etv1*, *Hes1*, *Nrf1*, *Nr2f2*, *Nupr1* and *Prdm16*) and examined their involvement in FGF8b mediated *Ucp1* expression by dsiRNA mediated gene silencing. Of the ten transcription factors, knockdown of only two transcripts significantly blunted (*Nrf1*) or completely abrogated (*Hes1*) the effect of FGF8b on *Ucp1* transcription (Figure 9E). Thus, FGF8b induced *Ucp1* expression depends on at least two transcriptional regulators *Nrf1* and *Hes1*.

In summary, FGF8b strongly induced *Ucp1* expression in a dose-dependent manner in white and brown undifferentiated preadipocytes. The signaling cascade was activated by binding of the FGF8b-heparin complex to FGFR1, the most abundant *Fgfr* gene in preadipocytes, and occurred via a MEK1/2-ERK1/2 axis. Paracrine fibroblast growth factors co-regulated PGE_2 production and glycolytic flux to control *Ucp1* expression and failure to induce either one of those two metabolic pathways prevented a full-scale induction of *Ucp1*. Lastly, the effect of paracrine fibroblast growth factors on *Ucp1* transcription in undifferentiated preadipocytes depended on the two transcriptional regulators *Nrf1* and *Hes1*.

4 | DISCUSSION

In the present study, we demonstrated that paracrine FGF8b is a strong inducer of *Ucp1* gene expression in cultured preadipocytes, and requires activity of two metabolic pathways, ie prostaglandin E_2 biosynthesis and glycolysis to act in concert.

Gene expression patterns induced by FGF8b and FGF9 are virtually identical (r = 0.999), suggesting that both paracrine FGFs share the same mechanism by which they regulate *Ucp1* expression. Shamsi et al, who investigated FGF6 and FGF9 mediated *Ucp1* expression in undifferentiated preadipocytes, identified PGE_2 biosynthesis to play a key role in the induction of *Ucp1*.[20] Similarly, our own data demonstrate that FGF8b increases prostaglandin metabolism, including *Pla2g4a*, *Ptgs2* (*Cox2*), *Ptges1*, *Slco2a1* expression and stimulates PGE_2 production (but not PGI_2) to regulate *Ucp1* expression. The fact that PGE_2 levels rise within hours upon treatment with FGF8b is indicative of a modulation of enzyme activity rather than expression levels in the first hours following treatment. Indeed, transcript abundance of *Ptges1*, the PGE_2 biosynthetic gene, starts to increase after this initial surge and this induction is even absent in brown preadipocytes derived from 129S mice, despite a dramatic upregulation of *Ucp1* (Figure S5A). Nevertheless, it is likely that changes in gene expression, particularly in the relatively rapidly induced expression of *Ptgs2*, help to sustain high levels of PGE_2 to overcome the short-lived effect of PGE_2 seen in cultured preadipocytes.

Interestingly, FGF8b induced PGE_2 biosynthesis has been demonstrated in rabbit chondrocyte cultures before,[38] lending additional support to a model in which FGF8b controls prostaglandin E_2 biosynthesis. A link between *Ptgs2* (*Cox2*) derived prostaglandins, including PGE_2 and PGI_2, and recruitment of beige adipocytes in WAT has been reported before.[35,36] Moreover, stimulation of undifferentiated SVF of WAT with PGE_2 and $cPGI_2$, a stable PGI_2 analog, for 3 hours induced *Ucp1* mRNA expression.[36] Given that FGF9 is released within BAT and WAT upon cold-exposure,[20] it is tempting to speculate that preadipocyte-specific and prostaglandin-dependent *Ucp1* expression contributed to the browning phenotype of WAT seen in those studies. Although PGE_2 alone was sufficient to induce *Ucp1* expression in preadipocytes, high micromolar concentrations of PGE_2 were required to elicit these effects. Possible explanations range from weak stability of PGE_2 under cell culture conditions, binding to serum albumin, which effectively reduces free PGE_2 concentrations, and unknown uptake kinetics hampering the comparison of endogenously produced prostaglandins with exogenously provided ones.

FGF8b treatment induced a very pronounced ECM remodeling effect in cultured preadipocytes, evident in changes in collagen biosynthesis related gene expression. Interestingly, FGF8b mediated degradation of ECM components and concomitant PGE_2 release occurs in rodent models of osteoarthritis and chondrocyte cultures, respectively.[38] Stimulation of human fat explants with PGE_2 significantly reduced the expression of fibrosis inducing genes.[39] FGF8b induced ECM remodeling may therefore be a direct consequence of the induction of PGE_2.

We here revealed an unexpected synergy of glucose metabolism and PGE_2 biosynthesis. FGF8b promoted glycolytic flux and impeding this flux through various means significantly blunted the effect of FGF8b on *Ucp1* expression, while PGE_2 production remained intact. Moreover, FGF1 failed to induce *Ucp1* expression despite comparably high elevation of PGE_2 levels in cell culture in response to FGF1 and FGF8b. Taken together, a pro-glycolytic state in preadipocytes appears to be a prerequisite for PGE_2 to upregulate *Ucp1* expression in a physiological setting. Notably, high glycolytic rates are a metabolic requirement for many highly proliferative cells, including cancer cells. The failure of FGF1 to induce *Ucp1* expression coincides with its relatively weak mitogenic activity in brown preadipocytes compared to FGF8b and FGF9 (Figure S1C). Hence, the upregulation of *Ucp1* by paracrine FGFs may be specifically linked to the metabolic demands of highly proliferative cells. The transcriptomic analysis revealed that the FGF signaling activity evoked by FGF1 is much lower than upon treatment with FGF8b, which indicates a potential point of divergence upstream of the signaling pathway. It is therefore conceivable that the difference between FGF1 and FGF8b in terms of biological potency may be caused through interactions with FGF-binding molecules, which result either in the inactivation of FGFs by sequestration or confer resistance to thermal or proteolytic degradation in cell culture media. In fact, one FGF8-binding protein present in preadipocytes is Fibulin-1, which has been shown to sequester FGF8, thereby suppressing FGF signaling.[40] Expression levels of Fibulin-1 were indeed significantly higher in control and FGF1 treated preadipocytes than in FGF8b or FGF9 treated preadipocytes according to our transcriptomic data, potentially reducing FGF1 signaling activity. This highlights the potential role of FGF-binding molecules, heparin included, in modulating FGF signaling activity.

The present work established that FGF8b induced *Ucp1* expression relied on *Fgfr1*, the most abundantly expressed *Fgfr* gene in brown and white preadipocytes. We showed that DsiRNA mediated loss-of-function of *Fgfr1* completely abrogated the effect of FGF8b on *Ucp1* expression, thoroughly examined potential cross-reactivities of employed DsiRNAs and presented data on FGFR1 protein knockdown efficiency. In contrast, Shamsi et al proposed the involvement of *Fgfr3* to mediate the effect of FGF6 and FGF9 on *Ucp1* expression in brown preadipocytes. While different FGFs may very well signal via different FGFRs, the remarkable overlap of gene signatures induced by FGF8b and FGF9 in our own work renders this scenario rather unlikely. In fact, we demonstrated that FGF6, FGF8b and FGF9 induced *Ucp1* expression to similar degrees in our own brown preadipocyte cell line, which barely expresses any *Fgfr3*. In addition, gene expression levels of *Fgfr1* and *Fgfr3* in the publicly available transcriptomic data linked to the study of Shamsi et al revealed that the *Fgfr1* gene is approximately 70-fold higher expressed than *Fgfr3*, demonstrating that *Fgfr3* is a low abundant *Fgfr* gene in preadipocytes.

The relative contribution of either *Fgfr1* or *Fgfr3* to paracrine induced *Ucp1* expression in preadipocytes thus remains to be unambiguously demonstrated in future experiments.

A significant upregulation of *Ucp1* in undifferentiated preadipocytes is difficult to reconcile with the traditional view of *Ucp1* function in thermogenic brite or brown adipocytes. The lack of abundant lipid droplets and no meaningful expression of beta-adrenergic receptors renders these cells dependent on the external supply of fatty acids to be thermogenically active. In fact, studies have shown that paracrine FGF induced UCP1 can be activated by exogenously supplied UCP1 activators such as perfluorooctanoic acid (PFOA).[20] Nevertheless, it is tempting to speculate whether the case of preadipocyte-specific *Ucp1* expression points towards a primarily non-thermogenic function in this cell type, for instance in response to cellular stress in control of redox homeostasis[37,41] or in defense against reactive oxygen species.[42,43] Further research is needed to determine the physiological relevance of this intriguing observation.

The focus of our study was the mechanism of *Ucp1* expression in the undifferentiated preadipocyte. To establish that this occurred in a preadipocyte-specific manner, we evaluated FGF8b treatment during differentiation of brown adipocytes (Figure S2A-C). FGF8b treated brown adipocytes were characterized by suppressed adipogenesis and lower *Ucp1* expression compared to the control group, despite an observed upregulation of *Ptgs2* (*Cox2*) and *Slc2a1*, indicating enhanced prostaglandin and glucose metabolism. Suppressed adipogenesis has also been observed as a result of FGF9 treatment during differentiation of adipocytes[20,21] and was associated with lower *Ucp1* expression.[21] Thus, the positive transcriptional regulation of *Ucp1* was not only independent of PPAR signaling, as shown earlier, but also only occurred in the absence of a general activation of the adipogenic transcriptional program in brown adipocyte cultures. The conflicting results between our studies in white epididymal adipocytes[23] and brown adipocytes can be resolved when their different intrinsic capacities for *Ucp1* expression are taken into account, and when the site of *Ucp1* expression is considered (adipocyte vs. preadipocyte). While the proliferation of preadipocytes with relatively high *Ucp1* expression can easily surpass *Ucp1* transcript levels of differentiated epididymal adipocytes, this does not apply to brown adipocyte cultures. Here, proliferation of the *Ucp1* positive preadipocyte fraction results in lower overall *Ucp1* expression, possibly due to the displacement of differentiated brown adipocytes. Taken together, these observations demonstrated that we found a unique system offering a tool to manipulate and understand *Ucp1* expression in preadipocytes, and potentially in non-adipocyte models.

In conclusion, we have experimentally established that FGF8b activated a FGFR1-MEK1/2-ERK1/2 axis to co-regulate two metabolic pathways, ie prostaglandin and glucose metabolism to control *Ucp1* expression. A coordinated

upregulation of the entire prostaglandin biosynthetic pathway via *Ptgs2* (*Cox2*) and *Ptges1* enabled a rapid surge in PGE_2 levels, constituting a necessary and to a lesser degree sufficient component in the induction of *Ucp1* expression. We showed that only in the presence of enhanced glucose uptake and high glycolytic flux, a full-scale induction of *Ucp1* materializes. Thus, an activation of glycolytic flux is required to act in concert with PGE_2 to maximally induce *Ucp1* expression in undifferentiated preadipocytes, a cell type formerly unrecognized as a source of *Ucp1* expression.

CONFLICT OF INTEREST

The authors declare that they have no conflict of interest.

AUTHOR CONTRIBUTIONS

T. Gantert conceptualized the study, designed experiments, performed the experiments, analyzed and interpreted data, including the RNA-Seq. experiments, and wrote the manuscript. C. Wurmser performed cDNA library preparation for the second RNA-Seq. experiment and provided the HiSeq2500 sequencing platform. L. Fischer performed preliminary experiments. J. Oeckl contributed to the methodology and interpretation of results. F. Henkel and J. Esser-von Bieren performed prostaglandin measurements and analyzed data. M. Haid and J. Adamski provided the analysis platform and assay for prostaglandin measurements. M. Klingenspor supervised the project and T. Fromme conceptualized and supervised the study and revised the manuscript.

DATA AVAILABILITY STATEMENT

The two transcriptomic data sets of this publication have been deposited to the NIH Gene Expression Omnibus (GEO) database with the following identifiers GSE168122 and GSE168124.

ORCID

Thomas Gantert https://orcid.org/0000-0002-0945-3167
Martin Klingenspor https://orcid.org/0000-0002-4502-6664

REFERENCES

1. Kajimura S, Saito M. A new era in brown adipose tissue biology: Molecular control of brown fat development and energy homeostasis. *Annu Rev Physiol*. 2014;76:225-249.
2. Bartelt A, Heeren J. Adipose tissue browning and metabolic health. *Nat Rev Endocrinol*. 2014;10:24-36.
3. Kajimura S, Spiegelman BM, Seale P. Brown and beige fat: Physiological roles beyond heat generation. *Cell Metab*. 2015;22:546-559.
4. Maurer S, Harms M, Boucher J. The colorful versatility of adipocytes: white-to-brown transdifferentiation and its therapeutic potential in man. *FEBS J*. 2020;1–19. https://doi.org/10.1111/febs.15470
5. Wu J, Boström P, Sparks LM, et al. Beige adipocytes are a distinct type of thermogenic fat cell in mouse and human. *Cell*. 2012;150:366-376.
6. Kozak LP, Koza RA, Anunciado-Koza R. Brown fat thermogenesis and body weight regulation in mice: relevance to humans. *Int J Obes*. 2010;34:S23-S27.
7. Cannon B, Nedergaard J. Metabolic consequences of the presence or absence of the thermogenic capacity of brown adipose tissue in mice (and probably in humans). *Int J Obes*. 2010;34:S7-S16.
8. Cypess AM, et al. Identification and importance of brown adipose tissue in adult humans. *Obstet Gynecol Surv*. 2009;64:519-520.
9. Van der Lans AA, Hoeks J, Brans B, et al. Cold acclimation recruits human brown fat and increases nonshivering thermogenesis. *J Clin Invest*. 2013;123:3395-3403.
10. Yoneshiro T, Aita S, Matsushita M, et al. Recruited brown adipose tissue as an antiobesity agent in humans. *J Clin Invest*. 2013;123:3404-3408.
11. Rosen ED, MacDougald OA. Adipocyte differentiation from the inside out. *Nat Rev Mol Cell Biol*. 2006;7:885-896.
12. Emanuelli B, Vienberg SG, Smyth G, et al. Interplay between FGF21 and insulin action in the liver regulates metabolism. *J Clin Invest*. 2014;124:515-527.
13. Fisher FF, Douris N, Fox EC, et al. FGF21 regulates PGC-1α and browning of white adipose tissues in adaptive thermogenesis. *Genes Dev*. 2012;26:271-281.
14. Ornitz DM, Itoh N. The fibroblast growth factor signaling pathway. *Wiley Interdiscip Rev Dev Biol*. 2015;4:215-266.
15. Itoh N, Ornitz DM. Evolution of the Fgf and Fgfr gene families. *Trends Genet*. 2004;20:563-569.
16. Itoh N, Ornitz DM. Fibroblast growth factors: from molecular evolution to roles in development, metabolism and disease. *J Biochem*. 2011;149:121-130.
17. Maddaluno L, Urwyler C, Werner S. Fibroblast growth factors: key players in regeneration and tissue repair. *Development*. 2017;144:4047-4060.
18. Degirolamo C, Sabbà C, Moschetta A. Therapeutic potential of the endocrine fibroblast growth factors FGF19, FGF21 and FGF23. *Nat Rev Drug Discov*. 2016;15:51-69.
19. Klein Hazebroek M, Keipert S. Adapting to the cold: a role for endogenous fibroblast growth factor 21 in thermoregulation? *Front Endocrinol (Lausanne)*. 2020;11:1-8.
20. Shamsi F, Xue R, Huang TL, et al. FGF6 and FGF9 regulate UCP1 expression independent of brown adipogenesis. *Nat Commun*. 2020;11:1-16.
21. Sun Y, Wang R, Zhao S, et al. FGF9 inhibits browning program of white adipocytes and associates with human obesity. *J Mol Endocrinol*. 2019;62:79-90.
22. Rulifson IC, Collins P, Miao L, et al. In vitro and in vivo analyses reveal profound effects of fibroblast growth factor 16 as a metabolic regulator. *J Biol Chem*. 2017;292:1951-1969.
23. Westphal S, Gantert T, Kless C, Hüttinger K, Klingenspor M, Fromme T. Fibroblast growth factor 8b induces uncoupling protein 1 expression in epididymal white preadipocytes. *Sci Rep*. 2019;9:1-11.

24. Tanaka A, Miyamoto K, Minamino N, et al. Cloning and characterization of an androgen-induced growth factor essential for the androgen-dependent growth of mouse mammary carcinoma cells. *Proc Natl Acad Sci U S A*. 1992;89:8928-8932.

25. Gemel J, Gorry M, Ehrlich GD, MacArthur CA. Structure and sequence of Human FGF8. *Genomics*. 1996;35:253-257.

26. MacArthur CA, Lawshé A, Xu J, et al. FGF-8 isoforms activate receptor splice forms that are expressed in mesenchymal regions of mouse development. *Development*. 1995;121:3603-3613.

27. Sunmonu NA, Li K, Li JYH. Numerous isoforms of Fgf8 reflect its multiple roles in the developing brain. *J Cell Physiol*. 2011;226:1722-1726.

28. MacArthur CA, Lawshé A, Shankar DB, Heikinheimo M, Shackleford GM. FGF-8 isoforms differ in NIH3T3 cell transforming potential. *Cell Growth Differ*. 1995;6:817-825.

29. Tacer KF, Bookout AL, Ding X, et al. Research resource: Comprehensive expression atlas of the fibroblast growth factor system in adult mouse. *Mol Endocrinol*. 2010;24:2050-2064.

30. Wang H, Willershäuser M, Karlas A, et al. A dual Ucp1 reporter mouse model for imaging and quantitation of brown and brite fat recruitment. *Mol Metab*. 2019;20:14-27.

31. Gaviraghi M, Vivori C, Pareja Sanchez Y, et al. Tumor suppressor PNRC 1 blocks r RNA maturation by recruiting the decapping complex to the nucleolus. *EMBO J*. 2018;37:1-18.

32. Mookerjee SA, Nicholls DG, Brand MD. Determining maximum glycolytic capacity using extracellular flux measurements. *PLoS One*. 2016;11:e0152016.

33. Mookerjee SA, Brand MD. Measurement and analysis of extracellular acid production to determine glycolytic rate. *J Vis Exp*. 2015;2:1-9.

34. Henkel FDR, Friedl A, Haid M, et al. House dust mite drives proinflammatory eicosanoid reprogramming and macrophage effector functions. *Allergy Eur J Allergy Clin Immunol*. 2019;74:1090-1101.

35. Madsen L, Pedersen LM, Lillefosse HH, et al. UCP1 induction during recruitment of brown adipocytes in white adipose tissue is dependent on cyclooxygenase activity. *PLoS One*. 2010;5:e11391.

36. Vegiopoulos A, Müller-Decker K, Strzoda D, et al. Cyclooxygenase-2 controls energy homeostasis in mice by de novo recruitment of brown adipocytes. *Science*. 2010;328:1158-1161.

37. Carrière A, Jeanson Y, Berger-Müller S, et al. Browning of white adipose cells by intermediate metabolites: an adaptive mechanism to alleviate redox pressure. *Diabetes*. 2014;63:3253-3265.

38. Uchii M, Tamura T, Suda T, Kakuni M, Tanaka A, Miki I. Role of fibroblast growth factor 8 (FGF8) in animal models of osteoarthritis. *Arthritis Res Ther*. 2008;10:1-10.

39. García-Alonso V, Titos E, Alcaraz-Quiles J, et al. Prostaglandin E2 exerts multiple regulatory actions on human obese adipose tissue remodeling, inflammation, adaptive thermogenesis and lipolysis. *PLoS One*. 2016;11:1-17.

40. Fresco VM, Kern XCB, Mohammadi M, Twal XWO. Fibulin-1 binds to fibroblast growth factor 8 with high affinity: effects on embryo survival. *J Biol Chem*. 2016;291:18730-18739.

41. Lagarde D, Jeanson Y, Barreau C, et al. Lactate fluxes mediated by the monocarboxylate transporter-1 are key determinants of the metabolic activity of beige adipocytes. *J Biol Chem*. 2021;296:1-14.

42. Oelkrug R, Goetze N, Meyer CW, Jastroch M. Antioxidant properties of UCP1 are evolutionarily conserved in mammals and buffer mitochondrial reactive oxygen species. *Free Radic Biol Med*. 2014;77:210-216.

43. Ježek P, Jabůrek M, Porter RK. Uncoupling mechanism and redox regulation of mitochondrial uncoupling protein 1 (UCP1). *Biochim Biophys Acta - Bioenerg*. 2019;1860:259-269.

SUPPORTING INFORMATION

Additional Supporting Information may be found online in the Supporting Information section.